University of Southampton

Set-up and Characterisation of an Electrospray Device and its Use for Particle Deposition

By Maria B. Gomis-Gomis

A thesis submitted in partial fulfilment for the degree of Master of Philosophy

in the
Faculty of Natural and Environmental Sciences
School of Chemistry

December 2014

Acknowledgements

I would like to thank my supervisor, Prof Jeremy Frey, for his assistance over the course of this higher degree. I would also like to express my sincerest thanks to Dr Adam R McKay, Dr Frutos Marhuenda-Egea and Mr Tony Longdon, for their time and advice. Finally, I would like to thank my family and friends, for their continued support and encouragement.

Abstract

This thesis documents the development of an EDS. The electrospray has been demonstrated to be a versatile technique with a broad range of applications. The methodology is broadly used for particle deposition or for production of liquid jets and droplets.

The device described in this work is used for on-demand preparation of samples that are suitable for CDI experiments, carried out on a table top XUV nanoscope. It is beneficial to have an ES device available to meet the specific requirements, (e.g., the size of the specimen, its shape, or an adequate substrate) for preparation of samples for imaging experiments because it would allow to have on-demand samples suitable for the development on the XUV nanoscope.

At the moment the electrospray device is used as EDS, but with the due modifications, it would be suitable as well for the production of liquid jets when it is required. The electrospray device will also contribute to sample fabrication for nano-objects imaging research work in the near future.

The configuration of the electrospray device comprises an electrospray emitter facing horizontally a grounded counter electrode. Alongside of this basic configuration, some peripherals such as an USB camera and a multimeter are included in order to monitor the electrospray process. For the deposition experiments the substrate is attached to the counter electrode, it will meet the liquid jet when the cone-jet spraying mode is achieved.

The development of the EDS involves its characterisation and optimisation, i.e., to evaluate the device performance for different experimental conditions in the order to find out the optimal conditions which lead to an stable spraying mode, generally the cone-jet

mode. It is found that the optimal conditions that lead to the production of a steady cone-jet spraying mode are as follows:

Applied voltage. 2.0kV

Distance emitter-counter electrode. 2.4–2.8mm

Flow rate. 400μL h^{-1}

ES emitter o.d./i.d. 360μm / 75μm

Liquid system. Methanol (LC-MS grade)

Due to the technical requirements of the table top nanoscope for biological imaging experiments, an isolated specimen of approximately 5μm must be deposited on a silica nitride window ($500 \times 500\mu$m square, 50nm thick). The specimen must retain its genuine structure after the spraying. Some diatom samples have been prepared using this ES head.

The samples have been successfully deposited onto glass and silica nitride windows. Visible from the SEM images are approximately 100nm diameter and approximately 500nm ridges in the diatom. Structure of such size is potentially resolvable using CDI with XUV radiation.

Acronyms

ASCII American Standard Code for Information Interchange

CCD Charge-Coupled Device

CDI Coherent Diffractive Imaging

CFEL Centre for Free-Electron Laser Science

CRM Charge Residue Model

DC Direct Current

DESY Deutsches Elektronen-Synchrotron

DNA Deoxyribonucleic Acid

DRAM Dynamics Random Access Memory

ED Electrospray Deposition

EDS Electrospray Deposition Source

EHD Electro-Hydrodynamic Deposition

EHDS EHD Source

ES Electrospray

ESI-MS Electrospray Ionisation Mass Spectrometry

FEL Free Electron Laser

FLASH FEL at DESY in Hamburg

IEM Ion Evaporation Model

LCLS Linac Coherent Light Source

LC-MS Liquid Chromatography Mass Spectrometry

LED Light-emitting Diode

LMIS Liquid Metal Ion Source

MS Mass Spectrometry

ORC Optoelectronic Research Centre

PCL Poly Caprolactone

PEG Polyethylene Glycol

Q-ToF Quadrupole ToF

SEM Scanning Electron Microscopy

ToF Time-of-Flight

UK United Kingdom

USB Universal Serial Bus

XFEL X-ray FEL

XUV eXtreme Ultraviolet

Contents

1 Introduction **13**
- 1.1 Motivation . . . 13
- 1.2 Thesis Aims . . . 15
- 1.3 Thesis Outline . . . 15

2 Background **17**
- 2.1 Introduction . . . 17
- 2.2 Electrospray Technique . . . 17
  - 2.2.1 Electrospray Stages . . . 18
  - 2.2.2 Onset Electric Field . . . 23
  - 2.2.3 Onset Voltage . . . 23
  - 2.2.4 Conductivity . . . 25
  - 2.2.5 Electrospray Characteristic Curves . . . 26
- 2.3 Electrospray Modes . . . 26
  - 2.3.1 Introduction . . . 26
  - 2.3.2 Dripping Mode . . . 27
  - 2.3.3 Micro-Dripping Mode . . . 28
  - 2.3.4 Spindle Mode . . . 28
  - 2.3.5 Multi-spindle Mode . . . 29
  - 2.3.6 Cone-jet Mode . . . 29
  - 2.3.7 Oscillating-jet Mode . . . 30
  - 2.3.8 Precession Mode . . . 30
  - 2.3.9 Simple-jet and Ramified-jet Modes . . . 30
  - 2.3.10 Multi-jet Mode and Rim Emission . . . 31
  - 2.3.11 Summary of the Electrospray Regimes . . . 31
- 2.4 Electrospray as a Sample Delivery System: Electrospray for Micro- and Nanoparticles Production and Delivery. . . . 34
  - 2.4.1 Introduction . . . 34

2.4.2 Electrospray Application in Life-Sciences . . . 34
2.4.3 Electrospray Application in Industry . . . 35
2.4.4 Electrospray Device Configuration and Performance . . . 36
2.5 Sample Delivery Systems Suitable for XUV and X-ray Scattering Experiments . . . 38

3 Experimental Design **40**
3.1 Introduction . . . 40
3.2 Configuration of an Electrospray Device . . . 40
3.3 Experimental Set-up and Data Processing . . . 41
3.3.1 Proposed Layout . . . 41
3.3.2 Electrospray Emitters Preparation and Testing . . . 45
3.3.3 Measurements . . . 46

4 Electrospray Device Optimisation **50**
4.1 Introduction . . . 50
4.2 Influence of Applied Voltage on Establishment of Cone-jet Mode: Onset Voltage . . . 50
4.2.1 Introduction . . . 50
4.2.2 Experimental Conditions . . . 51
4.2.3 Results and Discussion . . . 51
4.2.4 Conclusions . . . 55
4.3 Dependence of Spray Current on Flow Rate . . . 55
4.3.1 Introduction . . . 55
4.3.2 Experimental conditions . . . 56
4.3.3 Results and Discussion . . . 56
4.3.4 Conclusions . . . 61
4.4 Effect of Conductivity on Electrospray Current and Spraying Mode . . . 62
4.4.1 Introduction . . . 62
4.4.2 Experimental Conditions . . . 62
4.4.3 Results and Discussion . . . 63
4.4.4 Conclusions . . . 70

5 Electrospray Regimes **71**
5.1 Introduction . . . 71
5.2 Experimental Conditions . . . 71
5.3 Results and Discussion . . . 72
5.4 Conclusions . . . 75

6 CDI Sample Preparation **77**
6.1 Introduction . . . 77
6.2 Experimental Set-up . . . 77
6.3 Results and Discussion: Deposition Experiments . . . 78
6.3.1 Deposition of Gold Nanoparticles . . . 78

6.3.2 Deposition of Isolated Diatoms 80
6.3.3 Coherent Diffractive Imaging Experiments 84
6.4 Conclusions 86

7 Conclusion **89**
7.1 Electrospray Advantages 91
7.2 Electrospray Limitations 92
7.3 Electrospray Applications 92

A Appendix A **93**
A.1 Preliminary Instrumental Observations 93
A.1.1 Introduction 93
A.1.2 Effect of Microscope Lighting System on Temperature Around the Electrospray Emitter 93

B Appendix B **94**
B.1 Spray Current for Different Distances Between Tip of Capillary and Counter Electrode 94

List of Figures

2.1 Schematic of the electrospray process. A high voltage is applied between the spray emitter and the counter electrode. The high electric field in the vicinity of the emitter produce the migration of the liquid from the emitter tip to the counter electrode surface. 19

3.1 Schematic of the electrospray device. The voltage drop between the ends of the resistor is measured by using a multimeter with an Universal Serial Bus (USB)-computer interface. The data are logged to a computer and kept for later analysis together with the recorded images. 41
3.2 Photograph of the MicroTee® union. On the left-hand-side, the transfer capillary is linked to the syringe. On the right-hand-side, the electrospray emitter is placed opposite to the grounded stainless steel counter electrode. A platinum filament located inside the body of the MicroTee® union to establish the electric connection. 43
3.3 Photograph of the ED device. The MicroTee® union placed into the translating stage. This makes it possible to control the distance between the tip of the capillary and the counter electrode. The USB microscope is located above the tip and the counter electrode. 44
3.4 Details of the tapered capillaries. 46
3.5 Screenshot of the live video window. The text comments and the time stamps appear on the bottom left hand corner of the image. Software package is miXcope® 3.2.4. 47
3.6 Screen view of the intensity measurements. On the bottom left-hand-side, are displayed the collected data (voltages, time stamps, and the units (mV or V)). On the bottom right-hand-side, it is shown the XY graph area. In this zone are plotted the logged voltages (y-axis) against time (x-axis). . 48
3.7 Screen shots during data collection (left) and data analysis (right). . . . 49

4.1 Transition from micro dripping to cone-jet mode. In the case of the micro dripping mode, the meniscus is extended by a grey blurred zone (a), while in the cone-jet mode case, the contours of the jet and cone both appears well defined (b). 54
4.2 Spray current against time graph taken during an experiment. Similar curves are recorded for different flow rates 15μL h^{-1}, 50μL h^{-1}, 150μL h^{-1}, 300μL h^{-1}, 400μL h^{-1}, 600μL h^{-1}, and 800μL h^{-1} at different distances emitter-counter electrode, 0.4mm, 0.8mm, 1.2mm, 1.6mm, 2.0mm, 2.4mm and, 2.8mm. 57
4.3 Average spray current at different flow rates: 15 μL h^{-1}, 50 μL h^{-1}, 150 μL h^{-1}, 300 μL h^{-1}, 400 μL h^{-1}, 600 μL h^{-1}, and 800 μL h^{-1}, and distances emitter-counter-electrode 0.4 mm, 0.8 mm, 1.2 mm, 1.6 mm, 2.0 mm, 2.4 mm and, 2.8 mm. 58
4.4 Cone shape meniscus for 400μL h^{-1} at distinct distances. As the distance increases, once the cone-jet mode is achieved, the conical meniscus becomes sharper and the cone becomes better defined. At distances range from 2.4–2.8mm the cone appears stable and well defined. 59
4.5 Image of the cone-jet mode obtained with the electrospray device described in this work. The cone and liquid jet are illuminated with a green laser. This spraying mode is sustained for several minutes. 62
4.6 Intensity versus voltage curves at low voltages for a solution of methanol containing 0.10% of hydrochloric acid. 64
4.7 Meniscus shape for different applied voltages for the solution of 100% MeOH + 0.10% HCl. Figures 4.7(a), 4.7(b), 4.7(c), and 4.7(d) are the ES modes observed on the Dripping, pulsating area. Figures 4.7(e) and 4.7(f) are the ES modes observed in the Cone-jet area. Figures 4.7(g) and 4.7(h) are the ES modes observed on the Breakdown area. Magnification 60× 65
4.8 Intensity versus voltage curves at low voltages for a solution of methanol containing 0.25% of hydrochloric acid. 66
4.9 Meniscus shape for different applied voltages for the solution of 100% MeOH + 0.25% HCl. Figures 4.9(a), 4.9(b) and 4.9(c) are the ES modes observed on the Dripping, pulsating area. Figures 4.9(d) and 4.9(e) are the ES modes observed in the Cone-jet area. Figures 4.9(f), 4.9(g) and 4.9(h) are the ES modes observed on the Breakdown area. Magnification 60× 67
4.10 Intensity versus voltage curves at low voltages for a solution of methanol containing 0.50% of hydrochloric acid. 68

4.11 Meniscus shape for different applied voltages for the solution of 100% MeOH + 0.50% HCl. Figures 4.11(a), 4.11(b) and 4.11(c) are the ES modes observed on the Dripping, pulsating area. Figures 4.11(d) and 4.11(e) are the ES modes observed in the Cone-jet area. Figures 4.11(f), 4.11(g) and 4.11(h) are the ES modes observed on the Breakdown area. Magnification 60× 69

5.1 Spray current against time curve. The applied voltage increases in 0.5kV steps from 1.0–5.0kV. 72
5.2 Schematic of the spraying modes observed using the developed electrospray device. Depending on the flow rate the system evolves into dripping or micro dripping modes. As the applied voltage increases, for a steady flow rate, small but perceptible changes on the liquid meniscus occur developing the electrospray modes which start with the single cone-jet mode which evolves into the multi-jet and the rim emission modes. 73

6.1 Coated gold nanoparticles sprayed onto silica nitride. It is not possible to obtain isolated or evenly distributed specimens. The higher the similarity of the hydrophobicity of he coating and of the substrate, the higher the likelihood of an even particle deposition. 79
6.2 Slip set up. The glass slip is hold by a couple of plastic strips. It allows to move the slip up and down, on demand, in order to meet the liquid-jet. 81
6.3 Diatoms sprayed onto glass cover slip. Images taken from the same area, but with different magnification. The diatoms are distributed in groups, some isolated experiments can be obtained as seen in (c) 82
6.4 SEM images of a diatom specimens on glass. Images taken for the same zone but with different magnification. 83
6.5 Isolated specimen of a rectangular diatom sprayed onto a glass cover slip. Again, complex internal structure with holes and ridges. Images of the same specimen, but different magnification. 84
6.6 Optical transmission microscope image and SEM image of the diatom in a 10μm pinhole. 85
6.7 Visible from the SEM images are approximately 100nm diameter holes in the diatom and approximately 500nm ridges. Structure of such size is potentially resolvable using CDI with XUV radiation. 86
6.8 Reconstruction of the diatom image. 87

List of Tables

2.1 Summary of the spray modes. 33

4.1 Calculated E_{onset} for solutions containing different amount of methanol. Surface tension data taken from [79]. 52
4.2 Calculated $E_{capillary}$ for an applied voltage of 1.875kV. 52
4.3 Calculated E_{onset} for the solutions used in Set B. 53
4.4 Calculated $E_{capillary}$ for a distance of 0.8mm at some given voltages. . . 53
4.5 Spraying modes observed at different distances and flow rates. 60
4.6 Summary table of the experimental conditions which lead to the multi-jet spraying mode. 70

5.1 Physical properties of the solvent. Taken from [79]. 72
5.2 Summary of the electrospray modes observed. 76

7.1 Summary/Comparison of several EDS. 90

B.1 Spray Current measurements for 0.4mm gap 94
B.2 Spray Current measurements for 0.8mm gap 94
B.3 Spray Current measurements for 1.2mm gap 95
B.4 Spray Current measurements for 1.6mm gap 95
B.5 Spray Current measurements for 2.0mm gap 95
B.6 Spray Current measurements for 2.4mm gap 96
B.7 Spray Current measurements for 2.8mm gap 96

Chapter 1

Introduction

1.1 Motivation

X-ray crystallography is a nanoscale imaging technique that uses the diffraction of short wavelength light to obtain [1, 2] high resolution images. It is currently the principle method for structure determination of biological macromolecules such as large proteins, proteins complexes, and inorganic compounds. Although samples, such as proteins, have been studied [3] using this technique, the main limitation is that structure determination by X-ray crystallography depends on the process of protein crystallisation, e.g., the configuration/shape of the sample is often distorted, and there are many samples that cannot be crystallised due to their tendency to aggregate [4]. A method of imaging that is not limited in the same way would be beneficial to science.

Alternative techniques for nanoscale imaging, which allow for high penetration and high resolution, as well as removing the need of use crystallised samples. Using short-pulsed, spatially coherent XUV or X-ray light to scatter off samples is an alternative nanoscale imaging technique that allows high penetration and high resolution, as well as removing the need to use crystallised samples. Therefore an XUV/X-ray nanoscope could be an alternative to X-ray crystallography.

In order to obtain the highest possible resolution images, it is necessary to have high flux [5]. However, this can cause ionisation of inner electrons from atoms within a molecule. The repulsion between positively charged ions can cause a Coulomb explosion which results in irreversible sample damage [6]. The timescale of this damage is approximately 15fs (15×10^{-15}s) [5].

Neutze predicted [5] that by using femtosecond high intensity X-ray pulses with a wavelength between 2.33nm–4.37nm (water window). Since the water window is where the carbon in biological objects absorbs radiation strongly but the water does not, high contrast biological images are potentially producible.

By using an XUV or X-ray pulse that is temporally short, a scattering image of nanostructures can be recorded on a CCD camera before the sample is irreversibly damaged or destroyed [7]. CDI is a method that uses a phase retrieval algorithm to allow image reconstruction of a sample from the recorded scattering pattern [8, 9].

The development of a source of short pulsed high flux XUV or X-ray radiation, along with an appropriate imaging and sample handling setup, could potentially enable high spatial resolution images of nanoscale objects to be obtained.

To date, various sources exist for the generation of XUV and X-ray radiation. These include the FLASH FEL [10] at DESY [11] in Hamburg, the LCLS [12] in Stanford University and the UK Diamond Light Source [13] in Oxfordshire.

The FLASH FEL experiment reported [14] the first demonstration of ultrashort and extremely intense soft-X-ray scattering. A technology available on the scale of a table top could provide substantial benefits to the scientific community by offering a financially and more technologically accessible device.

A major experimental challenge for these XUV and X-ray radiation sources is sample manipulation and the delivery of macromolecules samples *in vacuo* at the interaction region. The sample delivery system needs to be optimised to achieve adequate particle densities so as to improve the image acquisition rate.

ES has attracted [15] recent research interest because it is an elegant and versatile way to make a broad array of nanoparticles. ES has three potential advantages. First, depending on the processing parameters, electrospray can generate monodisperse droplets whose size can vary from tens of nm to hundreds of μm. Secondly, it is a very gentle method since the free charge, induced by the electric field, only concentrates at the surface of the liquid, and does not significantly affect sensitive biomolecules such as DNA. Finally, electrospray has the ability to generate structured micro- and nanoparticles in controlled way.

For the advantages stated above, ES is a suitable technique for delivery (isolated particles, DNA, cells, etc.) and production of micro- and nanoparticles (spheres of polymers, encapsulations, etc.) of biological samples for CDI experiments. Several sample delivery

systems such as liquid-jets (Rayleigh Sources), aerosol stream and ion injection (ESI-MS for macromolecules) are under study for their use in the new European XFEL facility which is currently being developed [16].

At the ORC at Southampton University, Grant-Jacobs has developed [17] a table top nano scope. To test the this device and to further develop the concept, it would be necessary to also develop method to prepare suitable samples on-demand delivered on a silica nitride substrate.

This work will document the development of an electrospray head suitable for preparing samples for CDI experiments. These experiments will contribute to the development of a table top nanoscope, which will contribute to sample fabrication for nano-objects imaging research work in the near future.

1.2 Thesis Aims

In order to obtain high resolution images of biological samples, by CDI using the XUV light, it is necessary to have the specimen deposited on a suitable substrate. The particles under study must retain their native/genuine configuration.

Therefore, the aim of this work is to develop an electrospray source suitable for the preparation of on-demand samples that would be used in biological imaging. This would aid with the development of a table top XUV nanoscope.

1.3 Thesis Outline

The building of an electrospray head has several key aspects. This report focuses on the theoretical and practical process of setting up and optimising an electrospray device, and details the experimental process of using the electrospray technique for isolated particle deposition.

This thesis begins providing a background into the electrospray technique theory and experimental apparatus used to develop an EHDS or also called EDS. The process of electrospray is also discussed.

The spraying modes obtained with the proposed electrospray source are described and

analysed. The optimal working parameters for each spraying mode to emerge are determined.

The experimental work is discussed by investigating the effect of several working parameters on the electrospray device performance.

Finally, this work describes the experimental results obtained from the EHD of a diatom sample. This sample is used on CDI experiments. This thesis demonstrates the suitability of the proposed electrospray device for preparing on-demand samples for CDI experiments.

Chapter 2

Background

2.1 Introduction

In this section are described the ES methodology including the most important parameters involved in the electrospray process as well as the ES modes.

The electrospray technique is used in different ways, when applied in sample preparation/delivery systems such as liquid-jets, ion injection, and particle deposition. Some examples of applications are given as well as details of the electrospray technique in its broad range of application. It is explained as well its suitability for sample preparation, EDS, and/or sample delivery.

2.2 Electrospray Technique

The electrospray principle was reported [18, 19] by Zeleny at the beginning of the 20^{th} century. He showed that a liquid solution could be sprayed from a glass tube linked to a reservoir (where the liquid is kept) having a grounded plate located below the end of the glass tube by applying a high voltage at its outlet.

Since then, the electrospray technique has been developed and it is used, for instance, as an ionisation technique in MS. The ESI-MS is a gentle method which has the ability to produce intact ions with a wide variety of charge states. Under these soft conditions, weak bonds (such as non-covalent interactions) that exist in solution, can be preserved. It is suitable for the transfer of large compounds, like biomolecules, from the solution to

the gas phase.

By using the electrospray method, it is also possible to generate sub-μm jets and droplets. These can be directed by the electric field, which make the electrospray technique suitable for writing sub-μm patterns. It is a useful tool that is available to researchers who are involved in nanoscience and nanotechnology. It can be used for fabrication, dispersion, deposition and analysis of diverse nano-, bio-, and molecular materials [20].

2.2.1 Electrospray Stages

The electrospray is a technique where a solution is pumped through a capillary which is held at a high electric potential [21, 22]. The high voltage (2.0–5.0kV) is applied between a liquid in a thin capillary and a counter electrode. This high electric field between the tip of the capillary and the counter electrode creates a mist of highly charged droplets. A schematic of the electrospray process it is shown in Figure 2.1.

Usually, the electrospray process occurs at atmospheric pressure but, also, it is possible to use the electrospray technique in a vacuum. One of the severe problems in electrospraying liquids with high surface tension at atmospheric pressure is the corona discharge at the tip of the emitter [23]. This discharge causes the instability of the jet and the issue of poly disperse droplets. However, in a vacuum, the electric field is not limited by the appearance of corona discharges. Therefore, a molten metal (in LMIS)[1] and some organic solvents, having very high surface tensions, can be sprayed under a vacuum in a stable cone-jet mode. Recently, the interest of electric colloidal thrusters for spacecraft in using more conducting liquids, including glycerol, is increasing in the field of electric space propulsion [25, 26].

The mechanism of the electrospray can be divided [21] into three main steps:

1. The formation of charged droplets;
2. The solvent evaporation from charged droplets; and,
3. The formation of gas phase ions.

[1]LMIS is a device used to produce a beam of metal ions, charged clusters, or charged nanodroplets from a molten metal [24]. Metal beams are used in micro- and nanoelectronics for the production of thin metal films, ion deposition and implantation, mask less doping, and direct writing.

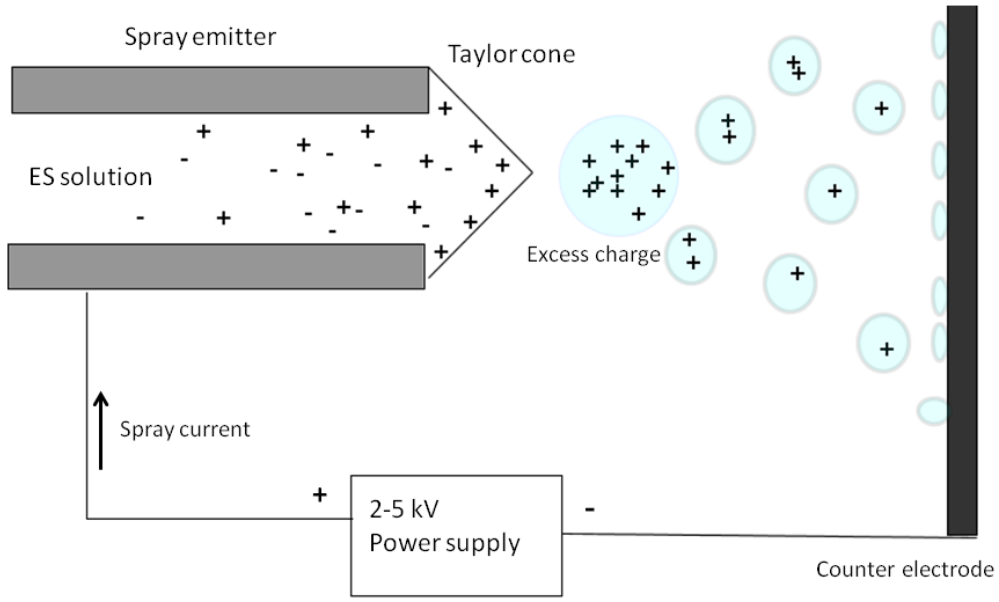

Figure 2.1: Schematic of the electrospray process. A high voltage is applied between the spray emitter and the counter electrode. The high electric field in the vicinity of the emitter produce the migration of the liquid from the emitter tip to the counter electrode surface.

The Formation of Charged Droplets at the Tip of the Capillary

A liquid sample is fed through a small capillary. The strong electric field applied between the tip of the capillary and a counter electrode produces a partial separation of positive from negative electrolyte ions in the solution. Assuming a positive potential (positive ion mode), the positive ions migrate away from the tip of the capillary towards the counter electrode, the negative ions migrate towards the inside of the capillary [27]. In the negative ion mode, the positive ions migrate towards the inside of the capillary, whereas the negative ions move towards the counter electrode. The equilibrium between different forces, such as:

- the repulsion of the positive charges accumulated at the liquid surface,
- the attraction of the positive ions by the electric field, and
- the surface tension of the liquid that provides a force to hold the liquid together,

causes the emerging liquid to elongate towards the counter electrode in what is known as a Taylor cone [28]. The tip of the cone, being the least stable point, elongates into liquid filament or jet, from which charged droplets are generated in a fine spray.

The spray generated is stable when the Taylor cone has a constant shape and has a continuous flow of droplets leaving from it. This is known as the "cone-jet" mode of operation. The stability of the electrospray depends on the ability to reach stable and effective spray conditions. In order to reach a stable spray mode, parameters such as the applied voltage, the solution characteristics (surface tension, viscosity and dielectric constant), the flow rate and the distance between the tip of the capillary and the counter electrode, have to be considered.

Solvent Evaporation from Charged Droplets Leading to Droplet Shrinkage and Coulomb Fission

When the charged droplets are travelling towards the counter electrode, they shrink, although the charge that they carry remains constant [29]. This leads to the increase of the electrostatic repulsion of the charges at the surface of the droplet. The maximum charge Q[N m V^{-1}] that the droplets can bear before their fission is given by the Rayleigh stability limit:

$$q_{R_g} = 8\pi(\epsilon_0 \gamma r^3)^{1/2} \tag{2.1}$$

Where ϵ_0, γ and r are the vacuum permittivity [NV^{-2}], the surface tension [N m^{-1}] and the droplet radius [m], respectively.

When the radius and charge both satisfy the Rayleigh stability limit (the point at which Coulombic repulsion of the surface charge is equal to the surface tension of the liquid), their fission in smaller droplets (offspring droplets) starts.

The time required for the first fission depends on the volatility of the solvent and on the droplet radius. The solvents with vapour pressure much lower than that for methanol will lead to acceptable ESI-MS sampling efficiencies only at elevated temperatures of the droplets and the ambient gas.

The radius of the small droplets (offspring droplets) is about one-tenth of the radius of the parents. They carry away only approximately 2% of the mass and 15% of the charge of the parent droplet. Subsequent fissions of the parent droplets are also shown. These occur at progressive shorter times, the time scale is hundred of μs. This time is not much shorter than the total residence time (which ranges from μs to a few ms) of charged droplets in the atmospheric pressure region of the ESI-MS device.

Formation of Gas Phase Ions

The ions contained in the charged droplets must be transferred into the gas phase in order to be detected and analysed by a mass spectrometer. It has been generally accepted that the solvent evaporates from the charged droplets until their charge density is high enough to allow their surface becomes unstable. There are two mechanisms proposed for explaining the formation of gas phase ions:

- Charge Residue Model (CRM), and
- Ion Evaporation Model (IEM).

The Charge Residue Model (CRM)

This mechanism was proposed [30] by Dole *et al.* when they reported about their work on analysing large molecules (Polystyrene 51,000 and 411,000 amu) by mass spectrometry.

The model was described as follows:

> *"By using electrospray it was thought that the drops on evaporation of the solvent would become electrically unstable and break down into smaller drops until possibly drops containing only the macromolecule per drop would result. On further evaporation of the solvent it was hoped to obtain electrically charged intact gas-phase macromolecules. It was thought that the charged drops would repel each other electrostaticaly and so prevent aggregation. It was also believed that the macroions so formed would be in a vibrational unexcited state and so not fragment."* [30]

At the time when Dole's group undertook their experiments, the large molecules that they were working on could not be transferred in to gas phase without damage and decomposition. Their aim was to obtain very small charged droplets retaining only one macromolecule (ions comprising a single macromolecule).

The Ion Evaporation Model (IEM)

Iribarne and Thomson [31, 32] based their theory on a derived equation that provides detailed predictions of the rate of ion emission from the charged droplets. At some point before a charged droplet becomes small enough to contain only one molecule, direct emission of ions from the droplets becomes possible. The charge density on the droplet surface becomes so high that the resulting field would be sufficiently intense to lead to the emission of one or more surface ions.

It has been suggested [33, 34] that both mechanisms apply, but for different types of analytes. In the case of very large species, such as PEGs with molecular masses as high as 5MDa or globular proteins (non denatured) [34] the CRM mechanism is the more likely ionisation scenario. However for smaller species like metal ions such as (Na^+, K^+) are more likely produced by the IEM mechanism.

2.2.2 Onset Electric Field

The value of the electric field at the tip of the capillary $E_{capillary}$ [V m^{-1}] can be evaluated using the approximate relationship,

$$E_{capillary} \approx \left(\frac{2V_c}{r_{ext} \ln\left(\frac{4d}{r_{ext}}\right)} \right) \tag{2.2}$$

where V_c [V], r_{ext} [m] and d [m] are the applied potential, emitter outer radius, and distance emitter-counter electrode, respectively.

Smith derived [35] the equation for the required electric field E_{onset} [V m^{-1}] at the tip of the emitter which leads to the instability of the static Taylor cone, and the formation of the charged jet,

$$E_{onset} = \left(\frac{2\gamma \cos 49.3^\circ}{r_{ext}\epsilon_0} \right)^{1/2} \tag{2.3}$$

where γ [N m^{-1}], and ϵ_0 [NV^{-2}] and r_{ext} [m] are the surface tension of the gas-liquid interface, vacuum permittivity, and emitter outer radius, respectively.

49.3° is the half angle of the Taylor cone; the unique solution to the $P\left(\frac{1}{2}\right)$ Legendre polynomial.

Taylor [28] was the first to demonstrate that the conical interface between two fluids can exist in equilibrium in an electric field. Considering the ideal case of a cone with a straight generatrix, in which the hydrostatic pressure (pressure exerted by a fluid at equilibrium due to the force of gravity) is zero, he showed that this equilibrium is obtained only for a single value of the applied potential, when the half-angle at the apex of the cone is equal to 49.3°.

2.2.3 Onset Voltage

Under the denomination of onset voltage, V_{onset}, [V] is defined the voltage needed to establish a stable cone-jet mode. Smith defined [35] the voltage required for the cone-jet mode to start and derived its equation, combining the equations for the onset field, E_{onset} and the field at the tip of the capillary $E_{capillary}$.

$$V_{onset} = \left(\frac{\gamma r_{ext} \cos 49.3^\circ}{2\epsilon_0} \right)^{1/2} \ln\left(\frac{4d}{r_{ext}}\right) \tag{2.4}$$

where γ, ϵ_0, r_{ext} and d are the surface tension of the gas-liquid interface [N m^{-1}], vacuum permittivity [NV^{-2}], emitter outer diameter [m], and distance emitter-counter electrode [m], respectively.

Smith described [35] the effect of the surface tension on the electrospray process.

Surface Tension

As it is shown in Equation 2.4, V_{onset} [V] is proportional to the surface tension, γ [N m^{-1}]. The solvent with the highest surface tension is the most difficult to stretch into a cone-jet.

For liquids with high surface tension, such as water, the voltage necessary to reach the cone-jet mode was around 11.5kV reported [36] by Borra or 15kV reported [37] by Jaworek. Borra also reported that at applied voltages higher than 11.4kV a continuous glow discharge (corona discharge) was established around the liquid cone. The corona discharge occurs due to the threshold field of gas ionisation being reached before the threshold field of the cone-jet mode. Smith also derived [35] the equation that depicts the dependence of the electrospray current I [A] on the surface tension γ [N m^{-1}]:

$$I = \left(\frac{\gamma^{3/2}}{\rho K R_f^{1/2}} \right) \tag{2.5}$$

where ρ, K, γ, and R_f are density [Kg m^{-3}], electrical conductivity [S m^{-1}], surface tension of the gas-liquid interface [N m^{-1}] and the filament or jet radius [m], respectively.

The electrospray current measured should be proportional to $\gamma^{3/2}$.

The Corona Discharge

Regarding the applied voltage an upper boundary exists as a corona discharge, referring the electrical break down between the electrospray tip and the counter electrode which produces a characteristic glow. The luminous region assumes the form of a cone and/or jet, which has a similar pattern to the jet that is traced during continuous illumination.

If the threshold field of gas ionisation is reached before the threshold of the cone-jet mode, electrical discharges can prevent the establishment of the cone-jet mode. For a liquid with high surface tension, for example water (0.072N m^{-1}), the establishment of a steady spray is usually prevented by discharges developed in the air around the liquid. This corona discharge has been observed [36] in electrospray experiments using water at high applied voltages, greater than 10.0kV. In a vacuum, the electric field is not limited by the appearance of corona discharges. Some means to produce a stable cone-jet mode of water had been used. It was possible to reduce the ionisation around the liquid cone by using more insulating gases (e.g., SF_6 or CO_2) or, using very fine emitters (less than 50μm).

2.2.4 Conductivity

Smith reported [35] the effect of the conductivity on the electrospray current and on the size of the jet and the aerosol droplet size. As the conductivity increases, the size of the jet and the aerosol droplet decrease. For high conductivity liquids, $> 10^{-1}$ S m^{-1}, the effect of the conductivity tend to mask effects due to the surface tension where both may be expected to have influence.

Cloupeau and Prunet-Foch studied [38, 39] the cone-jet mode with liquids throughout the range of conductivities from 10^{-1}-10^{-9} S m^{-1}. They reported that the spray current varies from the nA, for low conductivity liquids, to a few tenths of μA for high conductivity liquids. Higher currents are observed only if spraying is accompanied by corona discharges.

The cone-jet mode may be obtained with liquids of a broad range of conductivities. It enables the production of aerosols within a very large range of average drop sizes. For liquids with relatively high conductivities, the jet formation zone is limited to the apex of the meniscus. The remaining surface is practically equipotential and an almost static equilibrium of forces exists at each point.

The cone can assume three different forms: linear sides, convex or concave. The conical meniscus was present for liquids of high conductivity $> 10^{-1}$ S m^{-1}. At very low conductivity $< 10^{-11}$S m^{-1}, the meniscus was convex near the capillary and concave towards its apex [35]. The shape of the cone depends on the release of charges due, for instance, to corona discharge on the vicinity of the apex. The jet flows along the capillary axis or deflects form it just on a small angle usually smaller than 10°.

2.2.5 Electrospray Characteristic Curves

Marginean *et al.* reported *"the electrospray characteristics curves"* [40], plotting the spray current as a function of applied voltage. In their work it is highlighted the importance of monitoring the spray current, which can provide valuable information regarding the electrospray operation. An electrospray operating in the cone-jet mode provides relatively large and stable spray current.

Three different areas are displayed on these curves:

Dripping, pulsating area. For low values of applied voltage, the spray current remains steady. At these voltages the liquid is kept at the tip of the capillary and, in some cases, a very low frequency dripping is observed.

Cone-jet area. The voltage is increased and an accentuated increase of the spray current is observed. Beyond this point, the liquid meniscus becomes conical shape. The stable cone-jet mode is achieved, the electrospray current remains steady. The voltage at this point is called the onset voltage, V_{onset}.

Breakdown area. At greater applied voltages there is an increment in the spray current intensity. This will lead to the breakup of the jet into droplets. This area is also known as the "breakdown zone".

2.3 Electrospray Modes

2.3.1 Introduction

As the applied high voltage increases (for a constant liquid properties and flow rate) the electrospray process goes through several visual and measurable differences which are defined as spray modes or regimes. The electrospray regimes can be classified following different criteria.

Some authors classify [41, 42, 43] the spray modes by the morphology of the meniscus and by the continuity of the flow of liquid through the meniscus. Other authors have proposed [44, 45] to distinguish and classify the spraying modes according to the geometrical shape of the jet, the manner by which the jet disintegrates into droplets (e.g., by varicose, kink or spiral instabilities), and the geometry which the sprayed aerosol assumes.

A more recent classification of the electrospray regimes [46] is based on electrospray current measurements. Juraschek and Rollgen classified the electrospray regimes in one non-axial regime (rim emission) and three axial regimes: axial I (burst), axial II (pulsating cone) and axial III (cone-jet mode also called stable cone). The current was monitored by means of a storage-oscilloscope. Current pulsations with amplitudes in the nano Ampere (nA) range could be resolved up to frequencies of approximately 1MHz.

Several research groups have tried to establish nomenclature for the variety of observed electrospray modes. The terminology currently in use was proposed mostly on descriptive basis by Cloupeau and Prunet-Foch [42], who identified dripping, micro dripping, spindle, cone-jet and simple or ramified jet electrospray regimes. Jaworek and Krupa [44, 45] added to the classification three new spraying modes: the precession mode, oscillating-jet mode and multi-spindle mode.

2.3.2 Dripping Mode

In the absence of an electric field, the liquid remains at the tip or flows drop by drop at the emitter, depending on the chosen flow rate range. The application of a DC high voltage, causes a rise in the emission frequency and a reduction in droplet size. The dripping mode is characterised by the production of large droplets. In general, drop diameter remains greater than that of the capillary, thus leading to the emission of large drops at low frequency. The emission of drops may occur at regular time intervals, without the creation of satellites, so that all the drops have the same size. However the primary droplets are sometimes accompanied by satellite droplets.

Jaworek and Krupa reported [44, 45] that at low voltages, the drops are formed as regular spheres. As the voltage increases, the meniscus elongates and the drop becomes smaller. For higher voltages, the meniscus assumes a hemispherical or an elongated ellipsoid shape. Cloupeau and Prunet-Foch suggested [41, 42] that the electric field at the end of the hanging droplet is sometimes sufficient to create a jet (following the same process as the cone-jet mode) and later emission of a multitude of small droplets. Even in the case of dripping mode the emission of droplets is far from always happening in the same way.

2.3.3 Micro-Dripping Mode

At low flow rates, a different type of drop by drop emission may occur. This dripping mode yields droplets with diameters smaller than that of the capillary outlet diameter. The liquid issuing from the capillary assumes the shape of a flat stable cone-like or a hemispherical meniscus. At the end of the meniscus, a single small droplet is formed [41, 42]. The droplet is detached from the meniscus, and it does not undergo further disruption. The micro dripping mode differs from the dripping mode in that the meniscus does not contract after the droplet detachment.

The establishment of the micro dripping mode is observed only for low flow rates. A characteristic feature of the micro dripping mode is that the micro dripping and the cone-jet modes can appear under identical experimental conditions. One spraying mode may replace the other, both of them being kept for an extended periods.

2.3.4 Spindle Mode

The production of droplets could emerge from the breakup of a jet, or straight forward from the detachment of part of the liquid volume. In the spindle mode these two types of droplet production coexist.

Because of the shape of the jet emitted, this mode is referred as the spindle mode. When the voltage exceeds a certain critical value the regular spherical shape of the droplets (the dripping and the micro dripping modes) disappears and vast spindle-like fragments of liquid elongated by electrical forces are emitted from the capillary tip.

Cloupeau and Prunet-Foch reported [41, 42] the different stages of drop formation. After the spindle detachment, the meniscus contracts to a hemisphere and a new spindle starts to be formed while the detached spindle breaks up into several smaller droplets of different sizes which disperse off the capillary axis.

The spindle becomes longer and less regular as the voltage increases. As a result, the diameter of generated droplets also increases. With further increase in voltage the spindle changes to the multi-spindle or oscillating jet mode.

2.3.5 Multi-spindle Mode

This spraying mode was reported [45] by Jaworek and Krupa. The liquid is sprayed in spindle-like pieces of liquid similarly to the spindle mode. The meniscus at the tip of the capillary is flat and only a single small piece of liquid, usually in the form of a short spindle-like jet, is ejected at an instant from a distinct point at rim of the capillary. Although the multi-spindle mode resembles to some extent the multi-jet mode, they considerably differ from each other since the jet and the drop formation are different.

In the multi-spindle mode the liquid is not sprayed as a regular continuous thin jets, but as a spindle-like pieces of liquid. After its detachment the piece of liquid can disintegrate into a few smaller droplets. A few narrow streams around the capillary rim can be then distinguished. These streams of droplets, ejected periodically, seem to be distributed uniformly around the capillary edge.

The number of the emission points increases with the voltage increasing but only two to four such jets ejecting from the capillary were observed [45] in experiments with ethylene glycol. The generated droplets (few tens of μm in diameter) are greater than those in the multi-jet mode, but smaller than those in the spindle mode.

2.3.6 Cone-jet Mode

This mode was observed [18] for the first time by Zeleny. It has been investigated by many authors and has been given various names. Generally, it is known as a cone-jet mode, which simply denotes the shape taken on by the liquid at the tip of the emitter [41, 42, 43]. It is mostly associated with the stable cone regime. The liquid forms a regular cone at the outlet of the capillary, from which a stable thin jet of diameter ranging from μm up to tens of mm emerges.

Breakup of Jets into Droplets

The jet issued from the apex of the meniscus breaks up into droplets by two mechanisms as a function of increasing potential, depending on the amount of charge on a jet:

Varicose (axis symmetric) instabilities. The jet breaks into droplets which have similar size and sometimes accompanied by smaller satellite droplets.

Kink (off-axis) instabilities. For slightly higher voltages, lateral (or also called "whipping" instabilities) appear. The jet containing larger amount of charges, stretches out into disordered bending threads and is thinned out very irregularly. It breaks up into fine droplets of different sizes.

2.3.7 Oscillating-jet Mode

Once the cone-jet is achieved the increase in the flow rate allows the jet to become continuous. The intermittent drop generation is substituted by a continuous jet which oscillates or rotates because of the space charge of formerly emitted droplets and gas ions. In the oscillating-jet mode the jet issues smoothly from the meniscus at the tip of the capillary, and changes its position (oscillates) in one plane with the capillary axis [45]. The jet usually is not smooth, but becomes thinner at a few places. The jet disintegrates into small unequal droplets due to kink instabilities.

2.3.8 Precession Mode

This spray mode was characterised experimentally [47] by Jaworek and Krupa. It was documented photographically that the liquid issues from the capillary in form of a skewed cone which changes into a thin jet. The cone and the jet rotate around the capillary axis in a spiral-wise. The jet disintegrates into droplets at the distance about 5.0–10mm. The jet rotation is responsible for dispersing the droplets uniformly in a spraying cone with the axis co-linear with the axis of the capillary. With increasing voltage the jet becomes longer and rotates more regularly with 200–300 revolutions per second, for distilled water. As the voltage increases the droplet size distribution range (from 25–65μm) does not change significantly [45]. The advantages of the precession mode of spraying are the uniform spatial dispersion of the aerosol together with the similar droplet size distributions in each point of the spray cone.

2.3.9 Simple-jet and Ramified-jet Modes

These types of spraying were observed [41, 38] by Cloupeau. In these spray modes a continuous liquid jet emerges at the tip of the capillary. The ramified jet mode occurs at higher flow rates and it is characterised by one or more jets (primary jet(s)) emerging from the tip of the capillary. Several temporal secondary jets emerge from the surface

(not just from the apex) on the primary jets. Different varieties of this mode emerge as the applied voltage increases. This mode does not occur with water due to the initiation of corona discharges prevents reaching the electric field for the appearance of this mode.

2.3.10 Multi-jet Mode and Rim Emission

Multi-jet mode. When the voltage is gradually increased, the cone-jet may split with the meniscus forming two or more cones. Several emitting sites are then established around the edge of the capillary. The amount of jets increases with the applied voltage. This multi-jet mode makes it possible to obtain simultaneously a large number of jets on long circular or linear edges and, consequently, relatively high flow rates. Some authors consider [41, 42, 43] this mode as a mechanism for breaking up jet into droplets, but Jaworek and Kurpa identify [47] it as an independent spraying regime.

Rim emission. When more than five jets emerge, the multi-jet mode is called "rim emission". On this mode the droplets seems to be issued directly from the edge of the tip.

2.3.11 Summary of the Electrospray Regimes

In the following table, Table 2.1, are summarised the electrospray regimes and their properties. This classification was suggested [45] by Jaworek and Krupa. In general, the spraying modes can be divided into two groups.

The first group comprises the regimes in which only fragments of liquid (drops, droplets and spindles) are ejected directly from the meniscus at the outlet of the capillary. These regimes are the dripping, micro dripping, spindle, multi-spindle modes.

To the second group belong the modes in which the liquid emerges from the capillary in the form of a long continuous jet which disintegrates into droplets only in some distance, usually a few mm, from the tip of the capillary. These modes are: the cone-jet, precession, oscillating-jet, multi-jet and ramified-jet modes.

The jet, and also the meniscus, can be stable, can vibrate, rotate around the capillary axis or sometimes can whip irregularly. Although it is well known that the atomisation process is governed by the physical properties of the liquid (such as surface tension,

viscosity, density and conductivity) it also depends on the capillary diameter, its electric potential, and liquid velocity at the outlet of the capillary (volume and flow rate).

Table 2.1: Summary of the spray modes.

Spraying mode	Forms of liquid	Dynamics of meniscus / jet	Form of liquid emitted/ sprayed aerosol
Fragments of liquid (drops or spindles)			
Dripping	Meniscus: Semi-spherical Drop: Simple regular drop	Axially vibrating	Single drop
Micro-dripping	Meniscus: cone (linear or convex) Drop: Small spherical drop	Axially stable	Droplets accompanied with fine mist
Spindle	Meniscus: conical, semi-spherical Drops: elongated fragments of liquid (spindle)	Axially vibrating	Spindles accompanied with fine mist
Multi-spindle	Meniscus: flat Drops: multiple spindles	Steady/ lateral vibrating	Spindles around the edge breaking up into small droplets
Liquid jets			
Cone-jet	Semi-spherical meniscus	Axially vibrating	Simple regular drop, the sprayed aerosol is formed by a single drop
Oscillating-jet	Meniscus skewed, Jet: Linear.	Oscillating cone	Oscillating in a plane kink instabilities at end
Precession	Meniscus: Skewed,rotating cone Jet: Linear rotating around	Rotating around the capillary axis	Fine aerosol sprayed in a regular cone
Multi-jet	Meniscus: flat, with small cones on the rim Jet: linear, multiple	Stable	Fine aerosol sprayed in different directions
Ramified jet	Meniscus: irregular Jet: linear, ramified in random directions	Mother jet with randomly changed sub-jets	Droplets sprayed around capillary axis
Rim emission	Meniscus: flat Jet: linear, more than five jets	Stable	Fine aerosol sprayed in different directions

2.4 Electrospray as a Sample Delivery System: Electrospray for Micro- and Nanoparticles Production and Delivery.

2.4.1 Introduction

Electrospray is a critical element of ESI-MS, an analytical technique used to detect macromolecules that was developed [48, 49] by the 2002 chemistry Nobel Prize winner, Dr. John B. Fenn. Since then research has focused on developing an understanding of the process as well as exploring potential applications of electrospray in fields ranging from the semiconductor industry to life science.

2.4.2 Electrospray Application in Life-Sciences

Electrospray has been used to deposit particle suspensions to thin film [50, 24] or on-demand patterns, such as silica particle coatings on a quartz glass [20]. Various structured particles have been produced via electrospray, including poly(methyl-methacrylate)-pigment nanoparticles [51], cocoa butter microcapsules containing a sugar solution or an oil-in-water emulsion[52, 53], to name a few examples.

Moerman *et al.* produced [54, 55, 56] arrays of identical spots of 130–350μm in diameter consisting of biologically active substances, such as enzymes or antibodies, for the purpose of their use in medical diagnosis, environmental research, or combinatorial chemistry. The substances remained biologically active after electrospraying, provided that the current was lower than 500nA.

The electrospraying in the stable cone-jet mode allowed an accurate and reproducible dispersion of ultrasmall volume of liquid onto an array of spots without splashing, that is unobtainable by other deposition techniques, such as piezo dispensing or contact printing. Moerman *et al.* noticed that liquid droplets of a volume of 200pL (200×10^{-12}L) evaporate within 1s at room temperature upon landing onto substrate. Thus, a dry reagent dot is obtained that preserves protein stability. The enzymes sprayed on-chip (silica nitride) remained stable for a time of 45–60 days at a storage temperature of $-20°$C.

Uematsu *et al.* produced [57] biologically active protein thin films for protein-based biomaterials, biosensors and biochips. Tests indicated that the electrospraying had no

effect on biological activity of the proteins.

Electrospray has been used for medical applications. It has been successfully applied in tissue engineering, for instance, polymer materials including poly(lactide-co-glycolide) or poly(ethylene glycol) were electrospray-coated on biomedical implants [58].

In the area of drug/nucleic acid delivery, many biological materials, such as DNA, proteins, and lipids have been electrosprayed without changing their biological activity [59, 60, 61].

Proteins, such as bovine serum albumin, have been encapsulated in biodegradable polymeric microcapsules [62, 63] and small molecule drugs, and have been encapsulated in polymeric micro particles for systemic or oral delivery [64]

2.4.3 Electrospray Application in Industry

During the past two decades, electrospray has been used as well, for industry applications. It has been used to assist pyrolysis reactions and chemical vapour deposition processes, to produce inorganic particles including fine metal powder (Sn, Ag, Au, etc.), metal oxide particles (ZrO_2, TiO_2, etc.), ceramic particles (Si, SiO_2), and semiconductor quantum dots (CdSe, GaAs, etc.) [24, 20].

Some modifications on the electrospray set up could be done in order to improve the efficiency of the deposition. The use of hot plate surfaces as substrates is common for spraying processes for drying and/or pyrolysis of deposited droplets. It was reported that for deposition of metal oxides on a glass substrate [65], the deposition efficiency could be increased considerably while the electrical and optical properties of the deposited films could be maintained.

The electrospray technique has also been applied for producing thin films of ferroelectric $PbTiO_3$ on Si substrates [66] used in Dynamics Random Access Memory (DRAM)s, integrated optical devices, piezoelectric devices, and infrared sensors. Here the substrate temperature was 150°C. Other application is the preparation of nanocrystaline Pt thin films for exhaust gas treatment [67].

The ability to atomise a liquid sample into fL (10^{-15}L) droplets and deposit them on a surface is a key problem in micro fluidics and chemical analysis. A method to depositing fL droplets has been developed [68] by M.D. Paine's group. In this method is used nano electrospray to deposit small droplets onto a silicon surface which can be moved in order

to get control for the sprayed droplets. If the voltage is applied in short pulses the steady spray has been shown to deposit 0.3pL (0.3×10^{-12}L) droplets onto a substrate. If the number of pulses is too large, or the separation between deposition sites is too small, the deposited droplets coalesced into larger irregularly spaced deposits.

Compared with other film deposition methods, the electrospray deposition ED has the advantage of high deposition efficiency (up to 80%) as the droplets are transported by electrical forces and do not need a carrier gas (as in conventional sprays).

2.4.4 Electrospray Device Configuration and Performance

The electrospray process is easy to control by adjusting the liquid flow rate and the voltage applied to the emitter, and it is less expensive, for instance in production of thin films, than other deposition techniques such as chemical of physical vapour deposition or plasma spraying requiring high vacuum installations [24].

There are two main spray systems used for deposition:

- In the standard ES configuration, a simple nozzle (emitter) face the substrate. The high voltage is applied either to the emitter or the substrate, while the counter electrode is grounded. The substrate can be placed below the nozzle outlet, however, reverse configuration where the substrate is placed above the emitter, or systems with a horizontal emitter facing the counter electrode can be used as well. Other configurations based on some modifications of the standard configuration described above, are also possible. For instance, a coaxial electrospray configuration, where two liquids are fed through the inner needle and the outer needle, respectively. This configuration is widely used to produce structured nanoparticles, e.g, encapsulations. Multiplexed electrospray configurations have been developed [42, 45] to scale up production. The single needle is replaced by a micro-nozzle array. All nozzles work simultaneously and produce nanoparticles with the liquid flow injected through a needle by a syringe pump.
- Other possible configuration is the nozzle-extractor system, which operates independently of the substrate; the emitter is at high potential while the extractor (ring electrode) is located between the emitter and the substrate. The extractor electrode and the substrate are grounded.

The quality of the electrospray product depends on the interaction between the design

(emitter-substrate distance, emitter diameter and substrate temperature) and spraying parameters (liquid feed flow rate, applied voltage) as well as solution properties (concentration, viscosity, conductivity, density and surface tension). To improve and control the EDS performance it is important to understand the key parameters of the electrospray process and also the spraying modes. Some examples of the EDS uses are given as follows. These examples illustrate the role of the spray solution properties, the applied voltage and the design of the device.

For instance, the electrospray has been used [69] for the preparation of Poly Caprolactone (PCL) polymer particles with different microstructure. A PCL and chloroform solution with a concentration of 2 w/v % and 4w/v% was sprayed. As the concentration increased the pore size decreased, mostly range from 10-160nm. The porous microstructure is based upon phase separation. The polymer solution was placed in a 3.0mL syringe and was continuously pumped by the syringe pump at a flow rate of 3.0mL h^{-1}. The emitter is a stainless steel blunt nozzle with an internal diameter of 455μm, which was connected to the high-voltage power supply. The high-voltage applied is 8.0kV, potential difference between the nozzle and the grounded aluminium foil, which was placed on a lab jacket platform or immersed in a water bath around 5mm in depth, respectively. A spraying distance of 10cm between the nozzle and the collector was chosen for each set of experiments.

An interesting application of the EHD is for administering DNA-based therapeutics to the pulmonary epithelium. The effects of aerosolisation of naked or complexed DNA fragments via an electrospray on cells that had been cultured at an air-liquid interface, were studied [70]. The sprays have a high potential for delivery of DNA to the lungs tissue since damage to molecular integrity was minimal for all investigated DNA sizes.

Solutions (3.0mL) containing naked DNA or any of the suspensions were pumped through a stainless steel capillary (560μm i.d./1070μm o.d.) at a flow rate of 0.2mL/min using a syringe pump. The system, with a needle-to-ground distance of 2.5cm, was run at either a voltage of 0kV or -6kV. A dripping profile was observed at an applied voltage of 0kV while the applied voltage of -6kV exhibited a stable cone-jet.

The electrospray deposition of DNA solutions produces globular and fibrillar structures depending on the Electrospray (ES) conditions. Similar structures were observed [71] for both single- and double-stranded DNA molecules. Spraying under a positive potential from water solutions always resulted in formation of globules only. By contrast, ES from solutions under negative potential produced fibres and "pins" similar to those seen in

synthetic polymers.

An example of drastic changes in the electrospray deposition product with solvent and concentration is observed [71] in ES of DNA solutions: only globules are found after ES of 0.05mgmL^{-1} solution of λ-DNA in 85% acetonitrile whereas a solution of the same concentration in 90% of the same solvent produced numerous "pins" and extended fibres. No fibres were detected when λ-DNA was sprayed from water solutions.

2.5 Sample Delivery Systems Suitable for XUV and X-ray Scattering Experiments

The sample delivery techniques described below are included in the technical design report [16] for the development of the European XFEL Facility (XUV and X-ray radiation generation source) GmbH in Hamburg, Germany. At the time of writing the facility is under construction. It is expected to be finished by 2015.

Liquid-jet. Liquid-jet systems can produce stable Rayleigh droplet streams of particles in liquid suspension. Liquid-jets with diameters below 1μm have been developed [72] at Arizona State University. If a liquid is pressurised and forced though a small orifice into vacuum or stagnant air, the liquid emerges as a single continuos cylindrical liquid beam or jet.

The overall surface free energy of the jet is higher than that of an equivalent flow of spherical droplets. Consequently, the jet breaks up spontaneously at a certain critical distance downstream of the source aperture, producing a line of spherical droplets. The instability can be trigged by perturbing the source conditions at the frequency close to the intrinsic instability frequency. An example of a triggered process is the case of electrospray assisted (ES-assisted) Rayleigh sources, where an electrospray voltage is applied to the conventional source [72].

The droplet stream produced by the Rayleigh source have been successfully used for nano crystallography in many experiments [72] by Henry Chapman group at the LCLS at Stanford University, at FLASH FEL and at CFEL both located at DESY in Hamburg.

Aerosol stream. An aerosol sample injector allows the injection of droplets or dry particles from an aerosol into the vacuum chamber. This permits imaging of non-crystalline objects, such as single virus particles or biomolecules, with a consid-

erably reduced background compared to liquid-jet injection. Aerosolised samples will be injected in the vacuum through an aerodynamic lens stack. An injector has been developed [73] by Janos Hajdu's group at Uppsala University. The current prototype can focus particles of 3–3000nm diameter into a spot of a few μm. The design of the injector aims for the best possible performance for particles in the range of 10–600nm.

Ion injection. An additional system to deliver bio samples to the interaction region is by using an ion injector, implementing native MS as a method to deliver biological samples to the beam of the instrument.

In native MS, a mass spectrometer is used in conjunction with an electrospray source. This soft ionisation technique enables [74] the transfer of intact proteins and non-covalently bound protein complexes into the gas phase and subsequent structural analysis based on mass and shape of the ions.

Q-ToF mass spectrometers adapted for transmission of high-mass ions have become available during the last decade [75]. Differential pumping stages allow the ions to transit from atmospheric pressure to the vacuum of the mass spectrometer, providing a low background for X-ray scattering. Studies have shown that most protein complexes retain their structure upon charging and transfer into the gas phase.

In the first mass analyser, a quadrupole, ions can be selected according to their mass-to-charge ratio, or the entire ensemble can be transmitted. This allows the selective analysis of transient species in reactions, or the species of interest in a mixture. Detection of impurities from the production process can be avoided. After the quadrupole, the ions enter a collision cell. This cell can be changed to an ion trap to increase the ion density and function as an interaction region with the beam. Unused ions can be monitored in the final ToF mass analyser to verify their identity and the influx of particles from the electrospray source. The technique is also suitable for samples other than proteins, such as nucleic acids, organic polymers, and many more. The analytes can range from a few 100Da to several million Da, enabling studies on intact viruses [76, 77] with virtually no upper mass limit.

The systems described above are also substrate free.

Chapter 3

Experimental Design

3.1 Introduction

In this chapter we describe the EDS developed in this work. Together with the basic components of the device (emitter, power supply, counter electrode) a methodology is developed in order to observe (live), control and record the electrospray experiments to asses the device performance.

3.2 Configuration of an Electrospray Device

All the electrospray devices have components in common, these are:

Sample feeding system. It usually includes a syringe pump or a pressurised reservoir where the liquid to be sprayed is kept. The pressure in this reservoir has to be adjusted to deliver a suitable flow rate.

Emitter. The emitter is also called "electrospray tip" or "electrospray capillary". It can be made of conductive (stainless steel) or non-conductive (glass, fused silica) materials. The emitter tip shape (blunt or tapered) and its diameter (from 10μm to few mm) depend on the electrospray device. The emitter is connected to the power supply and to the sample delivery system.

Power supply. It should be capable of delivering voltages in the range of 0–10kV.

Counter-electrode. Depending on the design of the device, it could be a metal wire, a metal plate (aluminium, stainless steel). A flat grounded counter electrode is used

in the majority of the designs. It is located facing perpendicular to the emitter tip.

Together with these basic parts, it is necessary to observe whether or not the device is functioning properly, and which spraying regime is exhibited.

3.3 Experimental Set-up and Data Processing

3.3.1 Proposed Layout

Once we know the basic components of an electrospray device, it is decided to build up an electrospray device from scratch. The configuration of the electrospray device is similar to the standard electrospray [24] configuration described in Section 2.4.4.

The emitter is horizontally facing the grounded counter electrode surface.

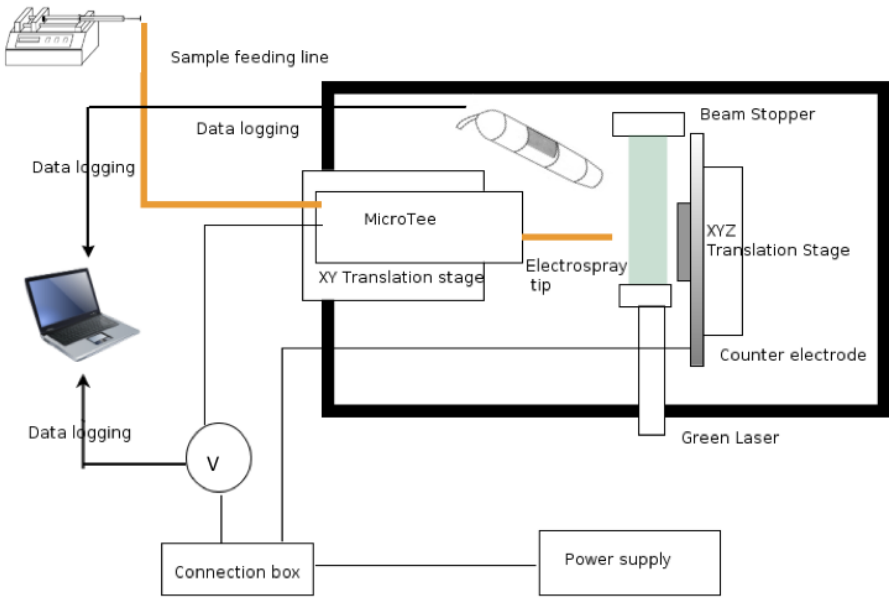

Figure 3.1: Schematic of the electrospray device. The voltage drop between the ends of the resistor is measured by using a multimeter with an USB-computer interface. The data are logged to a computer and kept for later analysis together with the recorded images.

A schematic of the electrospray device is displayed in Figure 3.1. The device is described as follows:

- The electrospray temitters (75μm i.d./360μm o.d., approximately 4cm long) are prepared by cleaving fused-silica capillary tubing. The details of the emitter preparation are described below in Section 3.3.2, as well as some experiments carried out to test home made against commercially available emitters. After the tests it is decided to use blunt emitters home made from fussed-silica capillary tubbing.
- The electrospray tip was connected to a transfer fused-silica capillary 75μm i.d./360μm o.d.
- The liquid is supplied via a 100μL syringe (Hamilton Bonaduz AG).
- A MicroTee® union (New Objective®) is the connection point for the electrospray voltage. MicroTee® union is shown in Figure 3.2.
- The liquid is infused by a syringe pump (KD Scientific, model KDS100) through the transfer capillary.
- The high voltages are applied to the emitter via a ISEG high voltage power supply (Model T2DP 0vv iii High Voltage Desk Top Power Supply).
- The output voltages range from 0–5.0kV.
- The location of the electrospray emitter is controlled by placing the MicroTee® union into a two axis translating mount (XY Translator, Throlabs Newton, NJ).
- Likewise, the counter electrode is also located in a XYZ translation stage.

The voltage drop across a 1MΩ high voltage resistor inline with the output of the power supply is measured in order to monitor the electrospray current.

The microscope is located as close as possible to the electrospray emitter. A green laser is used to illuminate the area around the tip of the capillary where the Taylor cone is produced. A photograph of the electrospray device set up is given in Figure 3.3.

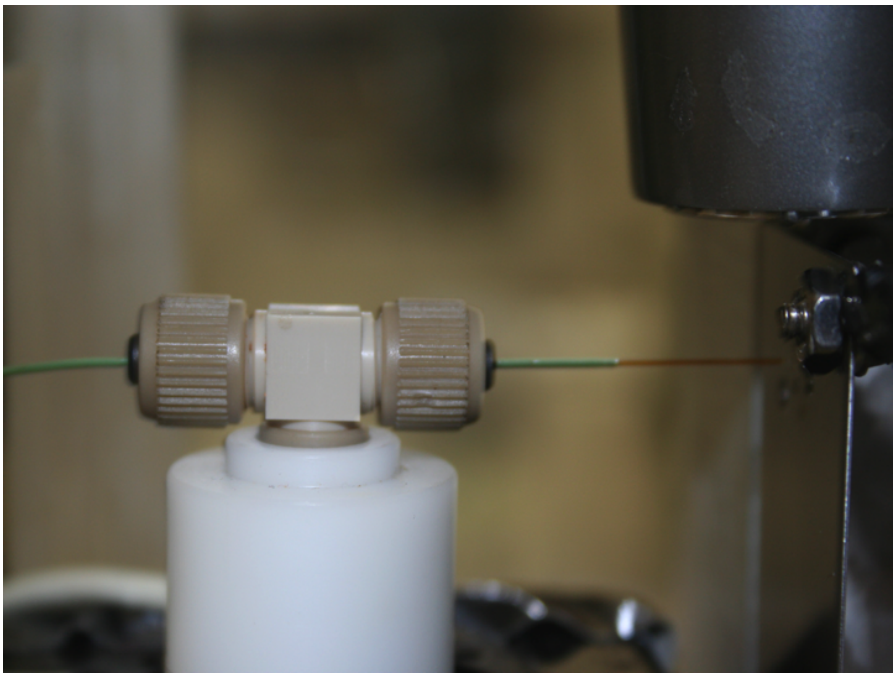

Figure 3.2: Photograph of the MicroTee® union. On the left-hand-side, the transfer capillary is linked to the syringe. On the right-hand-side, the electrospray emitter is placed opposite to the grounded stainless steel counter electrode. A platinum filament located inside the body of the MicroTee® union to establish the electric connection.

Figure 3.3: Photograph of the ED device. The MicroTee® union placed into the translating stage. This makes it possible to control the distance between the tip of the capillary and the counter electrode. The USB microscope is located above the tip and the counter electrode.

3.3.2 Electrospray Emitters Preparation and Testing

Electrospray Emitter Preparation

The electrospray tips or emitters can be tapered or blunt. The blunt tips are obtained by cleaving fused silica capillary tubbing using a diamond scribe. In order to obtain a distal and clean tip, the cleaving procedure has to be done very carefully. It is important not produce any flow-stopping particulate matter. The shape of the tip is inspected under the microscope before being used. The fabricated emitters are 4cm long, the fused-silica capillaries of different diameters are 20μm i.d./360μm o.d. and 75μm i.d./ 360μm o.d. The capillary puller available is the Sutter P2000®. This device is suitable for making tips for electrospray sources. The tapered tips can be produced by pulling fused silica capillary tubbing, the dimensions of the pulled tips would depend upon the dimensions (i.d./o.d.) of the fused silica tubbing. By adjusting some instrumental parameters, as explained on the capillary puller user's guide, tapered tips of approximately 13μm o.d., Figure 3.4(b), are obtained.

Electrospray Tip Testing

The different capillaries, blunt and tapered, are tested on the electrospray device spraying a filtered solution of methanol LC-MS grade.

In the case of the tapered capillaries, after being in use for a few minutes, the tip blocked and it could not be used again, despite using filtered LC-MS grade solvents. In Figure 3.4 are displayed some images of an experiment carried out with the tapered emitters, 13μm o.d.

The experiments carried out using blunt capillaries (75μm i.d./360μm o.d.) were replicated using the same tip several times. No signs of clogging are observed.

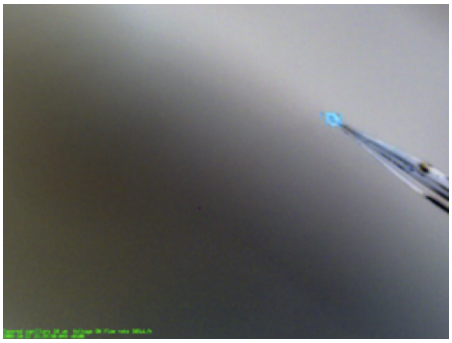

(a) ES applied voltage 2.0kV, flow rate 400μL h^{-1}.

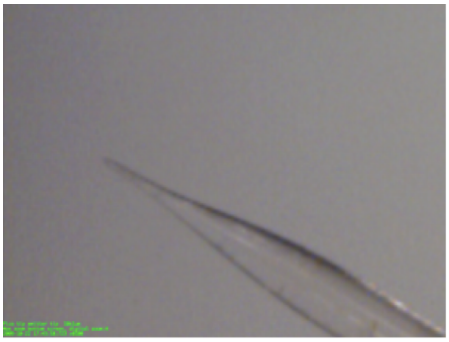

(b) ES emitter detail. Tapered capillary 13μm o.d.

Figure 3.4: Details of the tapered capillaries.

3.3.3 Measurements

Different diagnostic techniques are used to monitor the spray regimes: Observations of the liquid meniscus and spray current measurements.

Observations

A USB microscope (DinoLight® USB microscope) is used to record and observe the experiments at real-time. The microscope is located perpendicularly 1cm above the electrospray emitter. The effect of the microscope lighting system (LEDs) on the temperature around the emitter is explained in Appendix A. The magnification used is 60×. The software package miXcope®, enables the USB microscope for taking snapshots, recording movies, and measuring lengths and areas.

By using this software it is also possible to add time stamps and text comments, which appear in the live video window. A screen shoot of a live video window is given in Figure 3.5. Experimental details, such as flow rates, applied voltages or any other valuable information, can be attached as text comments.

Spray Current Measurements

The electrospray current I [A] can be defined as the charge streaming from the cone tip per unit time [78]. Spray current measurements are useful for diagnosing and figure out

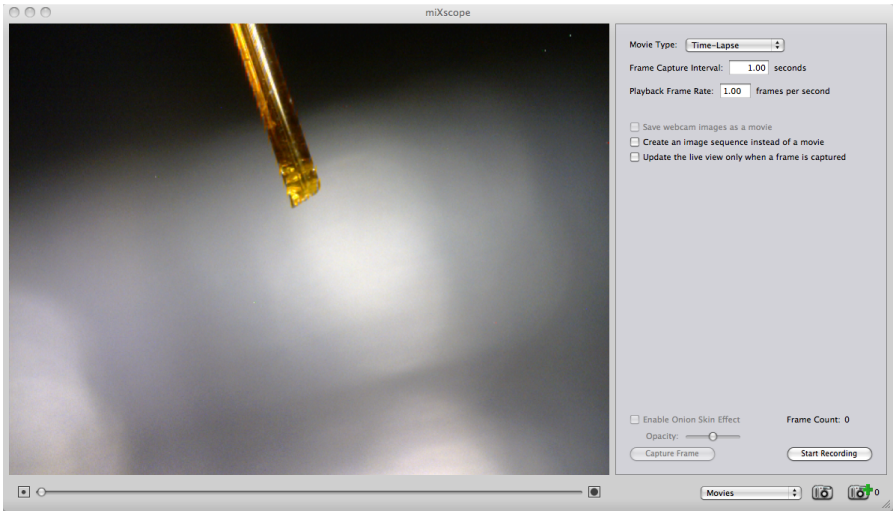

Figure 3.5: Screenshot of the live video window. The text comments and the time stamps appear on the bottom left hand corner of the image. Software package is miXcope® 3.2.4.

the complexities of the electrospray regimes. Although most commercial mass spectrometers monitor the spray current, this feature is almost never used for active control. Instead, the instrument parameters are usually tuned for the best possible ion current, and visual observation of the Taylor cone provides the comfort of using the electrospray in a regime that resembles the cone-jet.

To monitor the electrospray current, the voltage drop is measured across a 1MΩ high voltage resistor inline with the output of the power supply [1].

The measurements were taken through DC. A multimeter with USB-computer interface (Precision Gold, model N56FU) logged the voltage to a computer at a frequency of 1Hz.

The software package provided with the multi-meter is N56FU Communication Program V1.52, which displays data in a number of views, such as "XY graph" view and "Spreadsheet" view. The "XY graph" view displays the measured parameter against time. The "Spreadsheet" view displays text data in a format that can be easily copied and pasted into other applications. The data can also be saved to disk in standard ASCII text format. These views are available both during and after data collection. The data can be transferred (either as graphs or raw data) to other Microsoft Windows applications by using the clipboard (copy and paste).

[1] According to the Ohm's law, the potential difference (voltage) across a conductor is proportional to the current through it.

In Figure 3.6 it is shown a screen shot of the spray current data collection taken during an experiment.

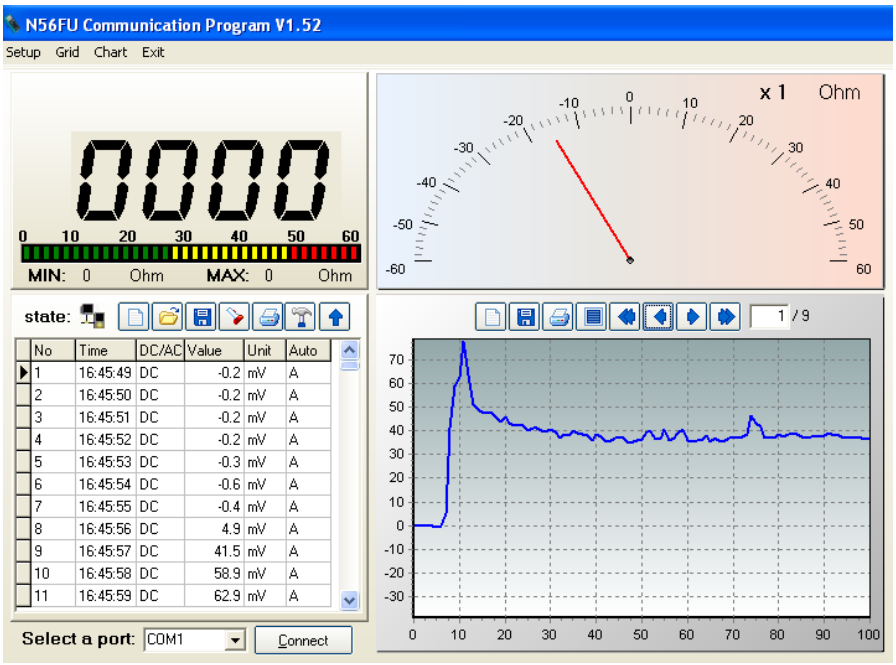

Figure 3.6: Screen view of the intensity measurements. On the bottom left-hand-side, are displayed the collected data (voltages, time stamps, and the units (mV or V)). On the bottom right-hand-side, it is shown the XY graph area. In this zone are plotted the logged voltages (y-axis) against time (x-axis).

The "XY graph" view a very useful feature, since it allows the observer to notice any fluctuations on the voltage drop which would indicate an anomalous behaviour on the electrospray. The data logging frequency can be modified, the maximum frequency allowed is 1Hz (one measurement per second). The data are saved in a spread-sheet. The time stamp (hh:mm:ss) that is given by the computer is used to launch and run simultaneously the software for both the multi-meter and the microscope.

Data Treatment

During each experiment it is possible to observe both the shape of the liquid meniscus and the voltage drop. The image shown in Figure 3.7(a) was taken during an experiment. On the bottom right, it is displayed how the voltages are plotted as they are collected and, on top left it is shown the live video window. In Figure 3.7(b) it is shown part of the data analysis process.

By recording the time stamp, each frame of any movie can be linked to the observed data. Events like the aggregation of liquid in the gap between the counter electrode and the emitter can be immediately noticed and associated to an unusual high value of the spray current.

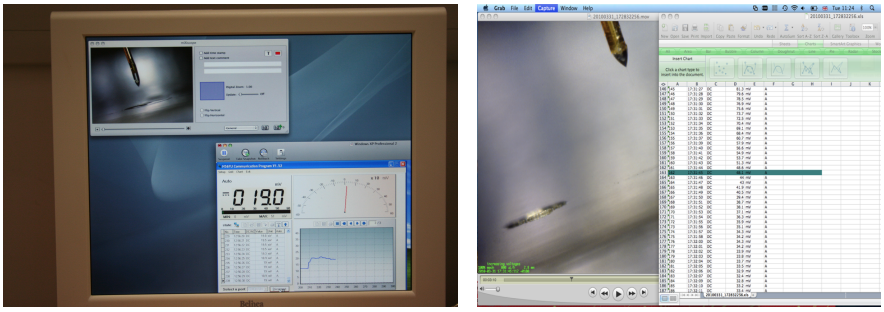

(a) View of an experiment and data recording.

(b) Screen shot during the data analysis.

Figure 3.7: Screen shots during data collection (left) and data analysis (right).

Chapter 4

Electrospray Device Optimisation

4.1 Introduction

In this chapter we explain some experiments carried out in order to determine the most suitable conditions to reach a stable spray mode, the cone-jet mode, in the electrospray device proposed in this work.

The device is tested under different experimental conditions, taking into account parameters involved in the electrospray process, such as surface tension, flow rate, conductivity and applied high voltage. The onset voltage will be determined as well as the effect of the surface tension and the distance of the emitter-counter electrode on the performance of the electrospray device.

4.2 Influence of Applied Voltage on Establishment of Cone-jet Mode: Onset Voltage

4.2.1 Introduction

Two sets of experiments, Set A and Set B, were carried out to determine the most favourable conditions regarding surface tension and distance emitter-counter electrode to reach a stable spraying mode.

4.2.2 Experimental Conditions

The experimental conditions for Set A were:

Liquid system. Water/methanol solutions. 0%, 10%, 20%, 40%, 60%, 80% and 100% (v/v) of methanol.

Distance emitter-counter electrode. It is successively increased from 0.4–4.0mm, in 0.4mm ± 0.016mm steps.

Applied high voltage. 1.875kV, kept for 2–4 minutes for each distance.

Flow rate. 15μL h^{-1}.

ES emitter o.d./i.d. 75μm i.d./360μm o.d., 4.1cm long.

For Set B, the experimental conditions were:

Liquid system. Water/methanol solutions 20%, 50%, and 80% (v/v) of methanol.

High voltage. It is applied in increments of 0.5kV and kept for 2 minutes, ranging from 1.0–3.0kV.

Flow rate. 15μL h^{-1}.

Distance emitter-counter electrode. 0.8mm.

ES emitter o.d./i.d. 75μm i.d./360μm o.d., 4.1cm long.

4.2.3 Results and Discussion

Set A

Regarding the effect of the distances between emitter-counter electrode on the spray current, it is observed that when the emitter is located at 0.4mm away from the counter electrode, even for low flow rates (5μL h^{-1}) the liquid accumulates in the gap. This leads to relatively high spray currents.

As the distance increases this effect becomes less perceptible, as expected, leading to lower spray currents. The main changes on the morphology of the liquid meniscus, described in Table 4.5, are observed at distances from 0.8–2.8mm. At greater distances, the liquid remains at the emitter tip and no changes in the meniscus are observed.

The E_{onset} for a given emitter outer radius, only depends on the surface tension of the liquid. In Table 4.1 we give the calculated values of the E_{onset}, for the aqueous mixtures of methanol (different surface tension) used in these experiments.

Table 4.1: Calculated E_{onset} for solutions containing different amount of methanol. Surface tension data taken from [79].

% Methanol	Surface tension / [N m^{-1}]	E_{onset} / 10^6 [Vm^{-1}]
0	0.0720	7.20
10	0.0562	6.35
20	0.0472	5.82
40	0.0365	5.12
60	0.0298	4.62
80	0.0255	4.28
100	0.0225	4.02

In the Table 4.2 we give the calculated values of $E_{capillary}$, for the distance range from 0.4–4.0mm.

Table 4.2: Calculated $E_{capillary}$ for an applied voltage of 1.875kV.

Distance / 10^{-3} [m]	0.4	0.8	1.2	1.6	2.0	2.4	2.8	3.2	3.6	4.0
$E_{capillary}$ / 10^6 [V m^{-1}]	9.53	7.23	6.34	5.83	5.49	5.23	5.04	4.88	4.75	4.64

A priori, based on $E_{capillary}$ and E_{onset} calculations for an applied voltage of 1.875kV it should be possible to reach a stable cone-jet mode, at the considered distances, from 0.4–4.0mm by using liquids which surface tension lies below 0.0298N m^{-1}, in other words, solutions containing more than 60% of methanol.

In practice, it is observed on the experiments that it is not possible to reach any stable spraying mode at any of the distances stated above. It is necessary to increase the applied potential in a few hundreds volts (in this case from 1.875–2.200kV) in order to observe any stable spraying mode, as it is shown below in Set B. This observation meets the conclusions reported by Smith [35] and Ikonomou [80] on their experimental verification of V_{onset}, $E_{capillary}$ and E_{onset} equations. They reported that for the stable operation of the cone-jet mode (steady conical meniscus, jet and spray) it is need to go few hundred volts higher than the V_{onset}.

Regarding the spraying modes exhibited, as the surface tension decreases, the dripping mode, low frequency spindle mode and unstable cone-jet mode emerge successively at distances range from 0.8–2.8mm.

Set B

As suggested by Equation 2.3, the lower surface tension, the lower E_{onset} and the lower onset voltage for the establishment of the cone-jet mode. In the Table 4.3 we give the electric field onset values of the solutions used in Set B.

Table 4.3: Calculated E_{onset} for the solutions used in Set B.

% Methanol	Surface tension / [N m^{-1}]	E_{onset} / 10^6 [Vm^{-1}]
20	0.0472	5.82
50	0.0329	4.86
80	0.0255	4.28

In the Table 4.4 we give the values for the electric field at the capillary $E_{capillary}$ tip for a given applied high voltages.

Table 4.4: Calculated $E_{capillary}$ for a distance of 0.8mm at some given voltages.

Applied Voltage / [kV]	Calculated $E_{capillary}$ / 10^6 [V m^{-1}]
1.000	3.86
1.500	5.79
2.000	7.72
2.500	9.65
3.000	11.58

For an applied voltage of 2.0kV, the value of $E_{capillary}$ is higher than that for E_{onset}, so the cone-jet mode should emerge at this applied voltage. As discussed previously in this section, usually it is necessary to apply several hundred volts more to reach a stable cone-jet mode. In addition, Smith also reported [35] the "hysteresis phenomena" for the onset voltage. The observed "hysteresis phenomena" consist in that once the cone-jet mode is achieved, this mode is kept even when voltages lower than the onset voltage are applied.

In Set B, small but perceptible changes are observed in the meniscus shape. For the solution of lower surface tension, it was easy for the liquid meniscus to reach a conical shape for a given applied voltage. It was the case of the solution containing 80% methanol, it exhibited the cone-jet and multi-jet modes at 3.0kV, although they were not stable modes.

The spray modes observed spraying the solutions under study are described as follows:

For the solution of 20% of methanol which surface tension is 0.0472N m^{-1}, at the applied voltages of 1.0kV and 1.5kV, the liquid is mostly kept at the emitter tip, only very low frequency micro dripping is observed at 1.5kV. As the voltage increases, 2.0kV, 2.5kV and 3.0kV applied, the micro dripping mode emerges and, after a couple of minutes, it is observed the transition from micro dripping to intermittent cone-jet modes. This transition between spraying modes is described [42] by Claupeau.

Both spraying modes are displayed in the Figure 4.1. In the case of micro dripping mode, the meniscus consist of an extended grey blurred zone, Figure 4.1(a), while in the cone-jet mode case the contours of the jet and cone both appears in black, well defined and clearly contrasted, Figure 4.1(b). No other modes are observed for the range of applied voltages considered.

(a) Micro dripping mode. Magnification 60× (b) Intermittent cone-jet mode. Magnification 60×

Figure 4.1: Transition from micro dripping to cone-jet mode. In the case of the micro dripping mode, the meniscus is extended by a grey blurred zone (a), while in the cone-jet mode case, the contours of the jet and cone both appears well defined (b).

For the solution containing 50% methanol which surface tension is 0.03286N m^{-1} at 1.0kV the liquid accumulates at the tip, no dripping is observed. At 1.5kV the meniscus becomes slightly elongated, and very small droplets are ejected, the micro dripping mode is present. The intermittent transition between the micro dripping and the cone-jet mode emerges from 2.0kV. As the voltage increases, at 2.5kV the intermittent cone-jet mode predominates and, for higher applied voltages 3.0kV, the cone-jet mode evolves into the multi-jet mode. In this case two jets are observed.

For the solution of 80% methanol which surface tension is 0.0255N m^{-1} at 1.0kV the liquid remains at the capillary and no dripping is observed. The voltage is increased to

1.5kV and the micro dripping mode arise. The dripping frequency is higher than that observed with the former solutions of 20% and 50% of methanol. The aggregation of small droplets on the counter electrode surface leads to the fluctuations in the electrospray current that are observed during the experiment. At applied voltages of 2.0kV, the micro dripping mode becomes stable cone-jet mode, which evolves into the multi-jet mode at applied voltages of 2.5kV and 3.0kV.

4.2.4 Conclusions

For this electrospray head, using water methanol solutions, the onset voltage is 2.0kV. However, in practice, it is observed that it is necessary to apply a few hundreds of volts more to reach a stable cone-jet mode.

A suitable range of distances to observe spraying modes in this device lies from 0.8–2.8mm.

As expected, the lower the surface tension, the easier to reach an stable spraying mode. Some spraying modes emerged by spraying solutions containing more that 60% of methanol.

Once the cone-jet mode is achieved, it can be maintained at slightly lower applied voltages, "hysteresis phenomena" for the onset voltage.

As described in Section 2.3.3, it is possible to obtain a micro dripping mode when the flow rate is low enough. At a flow rate of 15μL h^{-1} this mode is observed in this electrospray device. Its main feature is the straight forward transition, without any intermediate steps, from micro dripping (blurry meniscus) to intermittent cone-jet mode (well defined contour cone).

4.3 Dependence of Spray Current on Flow Rate

4.3.1 Introduction

In this section we describe the curves of the spray currents versus time recorded for different flow rates and distances emitter-counter electrode, in order to find out which are the experiential conditions that lead to the most stable spraying mode (cone-jet mode, i.e., steady conical meniscus, jet and spray).

4.3.2 Experimental conditions

Applied voltage. 2.0kV

Distance emitter-counter electrode. 0.4mm, 0.8mm, 1.2mm, 1.6mm, 2.0mm, 2.4mm and, 2.8mm

Flow rate. 15μL h^{-1}, 50μL h^{-1}, 150μL h^{-1}, 300μL h^{-1}, 400μL h^{-1}, 600μL h^{-1}, and 800μL h^{-1}

ES emitter o.d./i.d. 360μm / 75μm (4.1cm long)

Liquid system. Methanol (LC-MS grade)

4.3.3 Results and Discussion

Several spray current versus time curves, as displayed in Figure 4.2, are recorded for each distance and flow rate.

In these curves, three different zones can be distinguished:

- The high voltage "ON" zone;
- The "PLATEAU" zone; and,
- The high voltage "OFF" zone.

The spray currents considered for the average out are in the plateau area (highlighted in the plot).

The mean of the spray currents for each experiment are tabulated and displayed in the Appendix B. In Figure 4.3 we plot the mean of the spray current against the flow rate at the considered distance.

Having a look at Figure 4.3 it is noticed that up a flow rate of 400μL h^{-1} the spray current is higher than expected. at the distances bellow 2.0mm. This is due to the liquid accumulation on the counter electrode surface, as noticed in previous experiments.

Flow rates greater that 400μL h^{-1} are not recommended for this electrospray device in order to avoid the likelihood of liquid accumulation at short distances. This effect is evident for distances between 0.8 to 2.0mm, as displayed in Figure 4.4. As the distance increases the cone-jet evolves from intermittent to stable mode, as well as the conical shape of the liquid meniscus becomes better defined. For a flow rate of 400μL h^{-1},

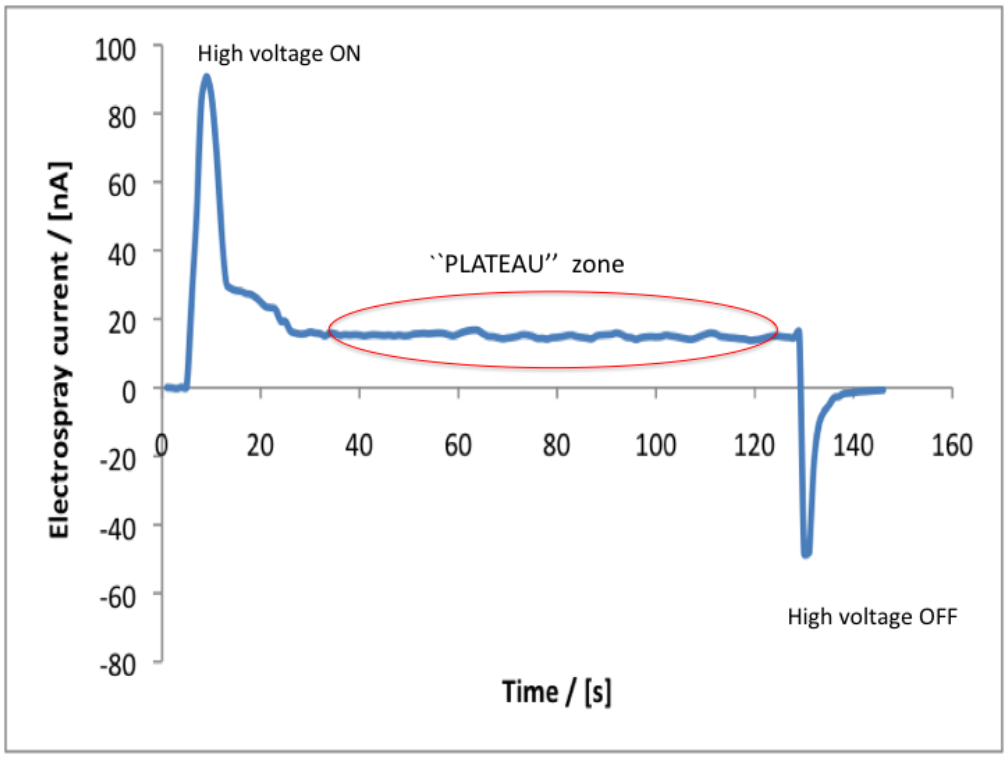

Figure 4.2: Spray current against time graph taken during an experiment. Similar curves are recorded for different flow rates 15μL h^{-1}, 50μL h^{-1}, 150μL h^{-1}, 300μL h^{-1}, 400μL h^{-1}, 600μL h^{-1}, and 800μL h^{-1} at different distances emitter-counter electrode, 0.4mm, 0.8mm, 1.2mm, 1.6mm, 2.0mm, 2.4mm and, 2.8mm.

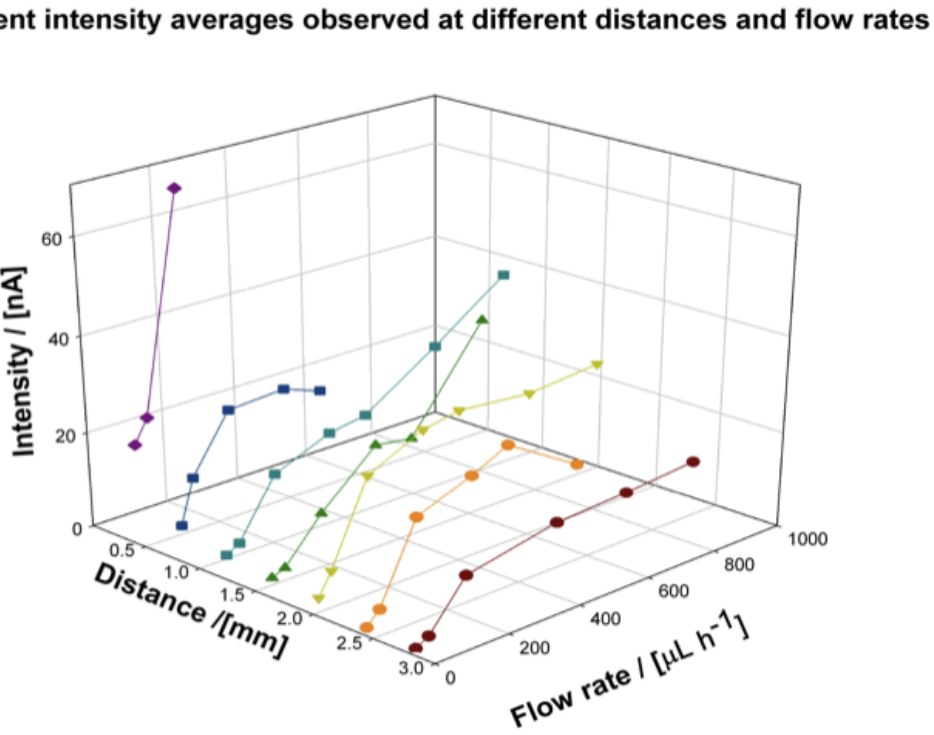

Figure 4.3: Average spray current at different flow rates: 15 μL h^{-1}, 50 μL h^{-1}, 150 μL h^{-1}, 300 μL h^{-1}, 400 μL h^{-1}, 600 μL h^{-1}, and 800 μL h^{-1}, and distances emitter-counter-electrode 0.4 mm, 0.8 mm, 1.2 mm, 1.6 mm, 2.0 mm, 2.4 mm and, 2.8 mm.

.

the better defined and more stable cone-jet modes emerge between 2.4–2.8mm. During the experiments it was observed that at the shortest distance between emitter-counter electrode, 0.4mm, the liquid remained in the gap even for low flow rates.

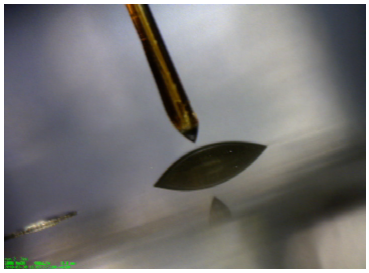

(a) 0.8mm. Magnification 60×

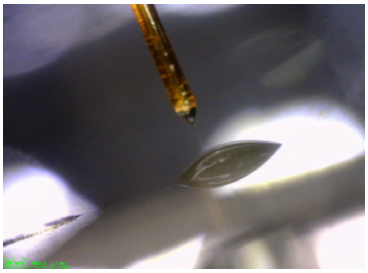

(b) 1.2mm. Magnification 60×

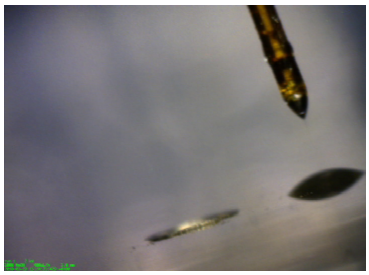

(c) 1.6mm. Magnification 60×

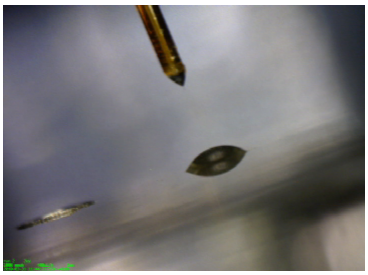

(d) 2.0mm. Magnification 60×

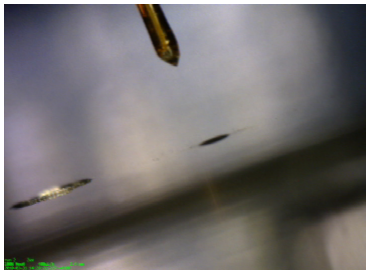

(e) 2.4mm. Magnification 60×

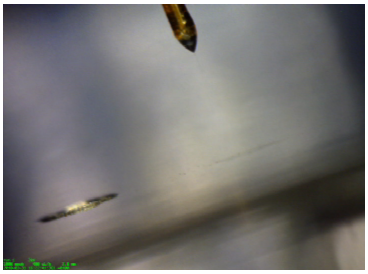

(f) 2.8mm. Magnification 60×

Figure 4.4: Cone shape meniscus for 400μL h^{-1} at distinct distances. As the distance increases, once the cone-jet mode is achieved, the conical meniscus becomes sharper and the cone becomes better defined. At distances range from 2.4–2.8mm the cone appears stable and well defined.

In Table 4.5, we summarise the spraying modes observed for each distance and flow rate.

Table 4.5: Spraying modes observed at different distances and flow rates.

Distance	0.4mm	0.8mm	1.2mm	1.6mm	2.0mm	2.4mm	2.8mm
Flow rate							
15[μL h^{-1}]	Liquid in the gap	Spindle	Microdriping	Microdriping	Microdriping	Microdriping	Microdriping
50[μL h^{-1}]	Liquid in the gap	Spindle	Microdriping	Microdriping	Microdriping	Microdriping	Microdriping
150[μL h^{-1}]	Liquid in the gap	Spindle to Intermittent Cone-Jet transition	Microdriping to Intermittent Cone-jet transition	Microdiping to Intermittent Cone-jet transition	Microdriping to Intermittent Cone-jet transition	Microdriping to Intermittent Cone-jet transition	Microdriping to Intermittent Cone-jet transition
400[μL h^{-1}]	No tested	Cone-jet (liquid on counter electrode surface)	Cone-jet (liquid on counter electrode surface)	Cone-jet (liquid on counter electrode surface)	Cone-jet (liquid on counter electrode surface)	Cone-jet	Cone-jet
600[μL h^{-1}]	No tested	Liquid in the gap	Liquid in the gap	Liquid in the gap	Liquid in the gap	Cone-jet	Cone-jet
800[μL h^{-1}]	No tested	Liquid in the gap	Liquid in the gap	Liquid in the gap	Liquid in the gap	Cone-jet (liquid on counter electrode surface)	Cone-jet

4.3.4 Conclusions

In these experiments we have learn that recording the spray current versus time curves in a useful tool to control the performance of the ES device. Any Irregular behaviour of the electrospray device, such as liquid accumulation on the counter electrode or an unexpected shortage on the liquid feeding system, has an effect on the spray current against time curves.

For this device an adequate distance emitter-counter electrode range from 0.8–2.8mm. Once the cone-jet mode is achieved the optimal distances are 2.4mm and 2.8mm. At these distances the cone-jet contour appears well defined and there is not liquid on the counter electrode surface.

The maximum flow rate which leads to a stable spraying mode in this electrospray source is 400μL h^{-1}.

The experimental conditions that give the most stable spray mode (cone-jet mode, i.e., steady conical meniscus, jet and spray) are:

Applied voltage. 2.0kV

Distance emitter-counter electrode. 2.4–2.8mm

Flow rate. 400μL h^{-1}

Liquid system. Methanol (LC-MS grade)

The conditions stated above have been tested several times. In all cases the cone-jet mode is observed, as shown in Figure 4.5. In order to improve the view of the cone and jet, a green laser is used to illuminate the area where the spray is produced.

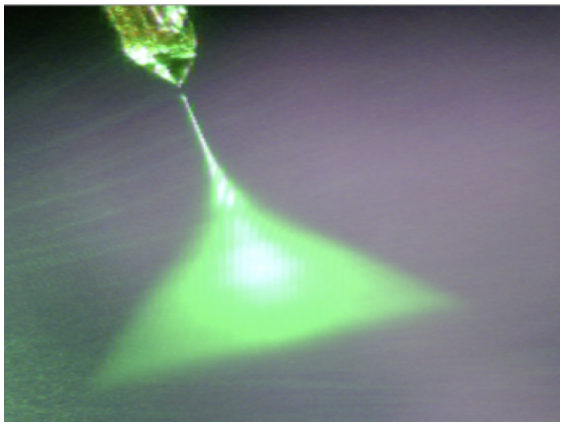

Figure 4.5: Image of the cone-jet mode obtained with the electrospray device described in this work. The cone and liquid jet are illuminated with a green laser. This spraying mode is sustained for several minutes.

4.4 Effect of Conductivity on Electrospray Current and Spraying Mode

4.4.1 Introduction

The effect of increasing conductivity on the electrospray regimes is studied by the addition to the liquid system (methanol) of a substance which is ionic in solution, hydrochloric acid. In this way, other liquid properties such as surface tension and viscosity were essentially constant, with only a small error.

In this section we describe the characteristics curves measured for liquid systems with increased conductivity. The changes observed in the liquid meniscus are attributed solely to changes in conductivity.

4.4.2 Experimental Conditions

Applied voltage. 1.0–2.6kV

Distance emitter-counter electrode. 2.4mm

Flow rate 400μL h^{-1}

Liquid System. Methanol (LC-MS grade)

The initial high voltage is set at 1.0kV and kept for two minutes. Then it is increased in 0.2kV steps also kept for two minutes. Around the onset voltage, 2.0kV, the voltage is increased in 0.1kV steps. Conductivity is increased by adding 0.10%, 0.25% and 0.50% (v/v) of hydrochloric acid.

4.4.3 Results and Discussion

Marginean *et. al* reported *"the electrospray characteristics curves"* [40]; plotting the spray current as a function of applied voltage. In their work, it is highlighted the importance of monitoring the spray current, which can provide valuable information regarding the electrospray operation. An electrospray operating in the cone-jet mode provides relatively large and stable spray current. The different areas of this curves are explained in Section 2.3.5.

The characteristic curves are recorded for methanol solutions with increased conductivity by the addition of hydrochloric acid, 0.10%, 0.25% and 0.50% respectively. In Figures 4.6, 4.8 and 4.10 are displayed the spray current against voltage profiles.

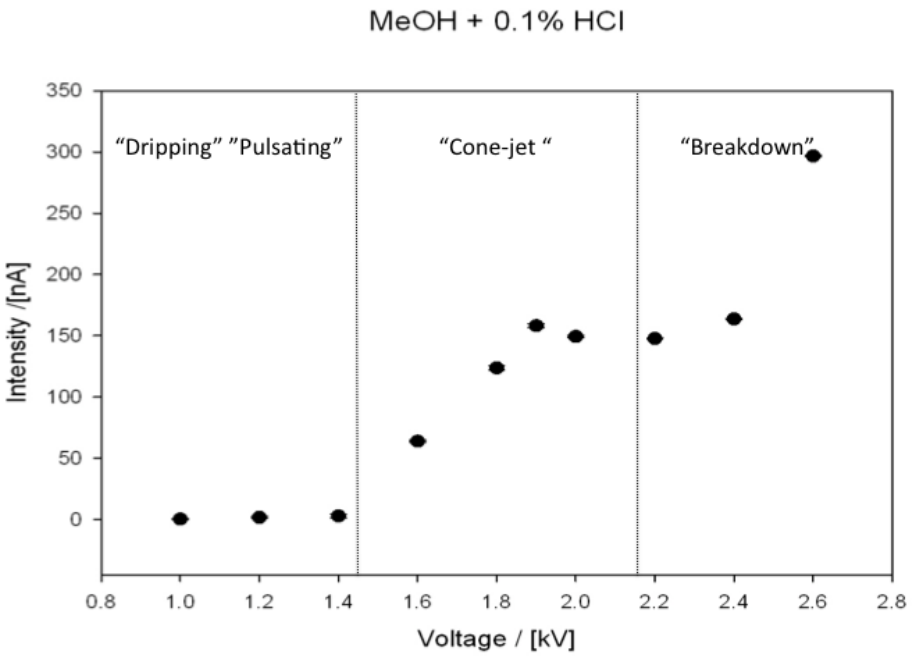

Figure 4.6: Intensity versus voltage curves at low voltages for a solution of methanol containing 0.10% of hydrochloric acid.

The electrospray modes exhibited with the solution of 100% MeOH + 0.1% HCl, are described as follows:

Dripping, pulsating area. At 1.0kV and 1.2kV, the liquid remains at the tip of the capillary Figure 4.7(a), and no dripping mode is observed. The dripping mode emerged at 1.4kV, Figure 4.7(b). At 1.6kV, Figure 4.7(c) and 1.8kV, Figure 4.7(d) the elongated meniscus with ejection of small droplets is present. This description corresponds to the spindle mode.

Cone-jet area. At 1.9kV, Figure 4.7(e) the meniscus remains elongated but its shape becomes conical at the tip. At 2.0kV, Figure 4.7(f) the cone-jet mode emerges.

Breakdown area. As the voltage increases the cone-jet mode remains but the cone tip become slightly off axis, Figure 4.7(g). This trend is increased with the voltage and leads to the multi-jet mode exhibited at 2.6kV, Figure 4.7(h).

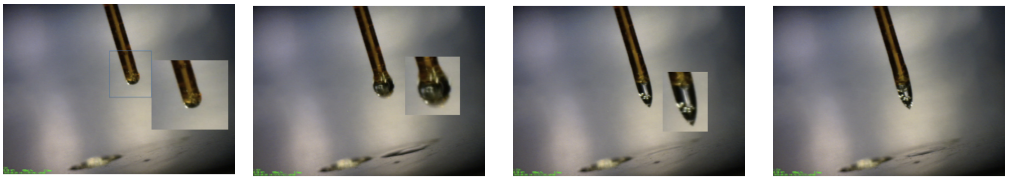

(a) 1.0kV and 1.2kV (b) 1.4kV (c) 1.6kV (d) 1.8kV

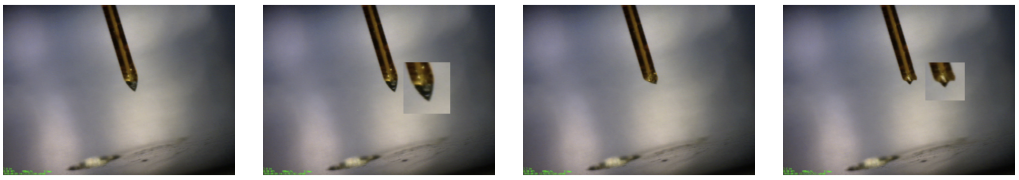

(e) 1.9kV (f) 2.0kV (g) 2.2kV and 2.4kV (h) 2.6kV

Figure 4.7: Meniscus shape for different applied voltages for the solution of 100% MeOH + 0.10% HCl. Figures 4.7(a), 4.7(b), 4.7(c), and 4.7(d) are the ES modes observed on the Dripping, pulsating area. Figures 4.7(e) and 4.7(f) are the ES modes observed in the Cone-jet area. Figures 4.7(g) and 4.7(h) are the ES modes observed on the Breakdown area. Magnification 60×

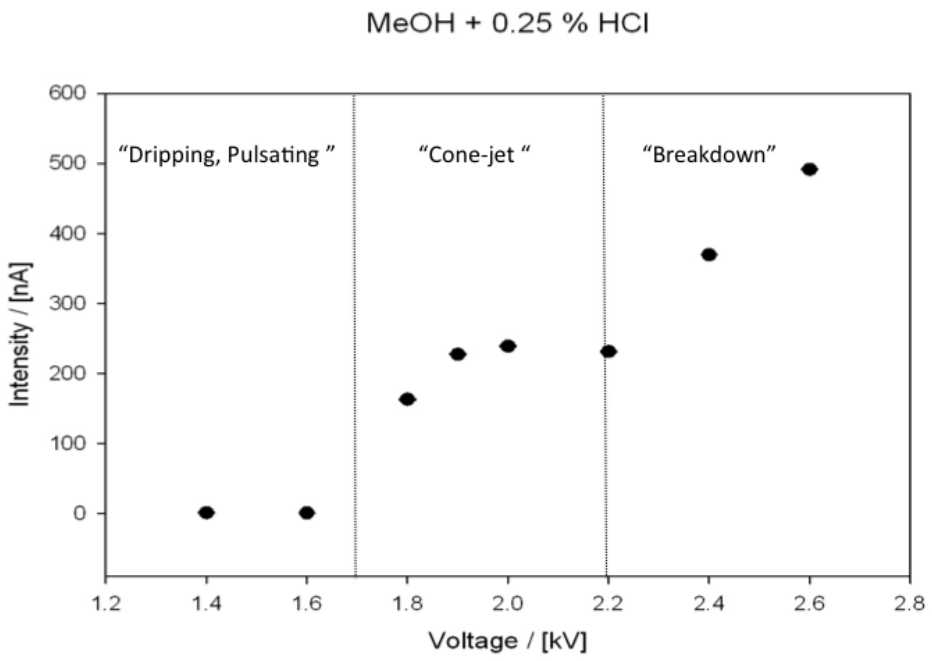

Figure 4.8: Intensity versus voltage curves at low voltages for a solution of methanol containing 0.25% of hydrochloric acid.

The spraying modes observed on the experiments are described below in Figure 4.9.

The conductivity is increased by adding hydrochloric acid, 100% MeOH + 0.25% HCl. The observed spraying modes are described as follows:

Dripping, pulsating area. At 1.0kV and 1.2kV, the liquid remains at the tip, Figure 4.9(a). At 1.4kV and 1.6kV, small droplets are ejected from the tip of the capillary, the meniscus kept its hemispherical shape after the droplets detachment, Figures 4.9(b), and 4.9(c).

Cone-jet area. At 1.8kV, the intermittent cone-jet mode emerges, Figure 4.9(d), and, at 1.9kV, the cone-jet mode attain its stable configuration, Figure 4.9(e).

Breakdown area. The intermittent multi-jet mode and off-axis instabilities are present at 2.0kV, Figure 4.9(f). At 2.2kV and 2.4kV, the multi-jet mode becomes more stable, two cones and two jets are observed, Figure 4.9(g). At 2.6kV, the multi-jets mode is still observable but the size of the cones is slightly smaller than that for

2.4kV, which indicates the transition to the rim emission mode as higher voltages are applied, Figure 4.9(h).

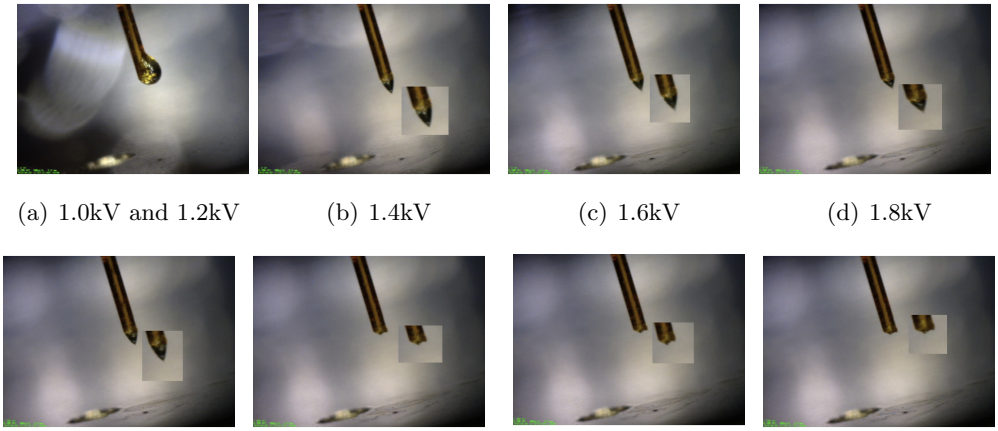

(a) 1.0kV and 1.2kV (b) 1.4kV (c) 1.6kV (d) 1.8kV

(e) 1.9kV (f) 2.0kV (g) 2.2kV and 2.4kV (h) 2.6kV

Figure 4.9: Meniscus shape for different applied voltages for the solution of 100% MeOH + 0.25% HCl. Figures 4.9(a), 4.9(b) and 4.9(c) are the ES modes observed on the Dripping, pulsating area. Figures 4.9(d) and 4.9(e) are the ES modes observed in the Cone-jet area. Figures 4.9(f), 4.9(g) and 4.9(h) are the ES modes observed on the Breakdown area. Magnification 60×

.

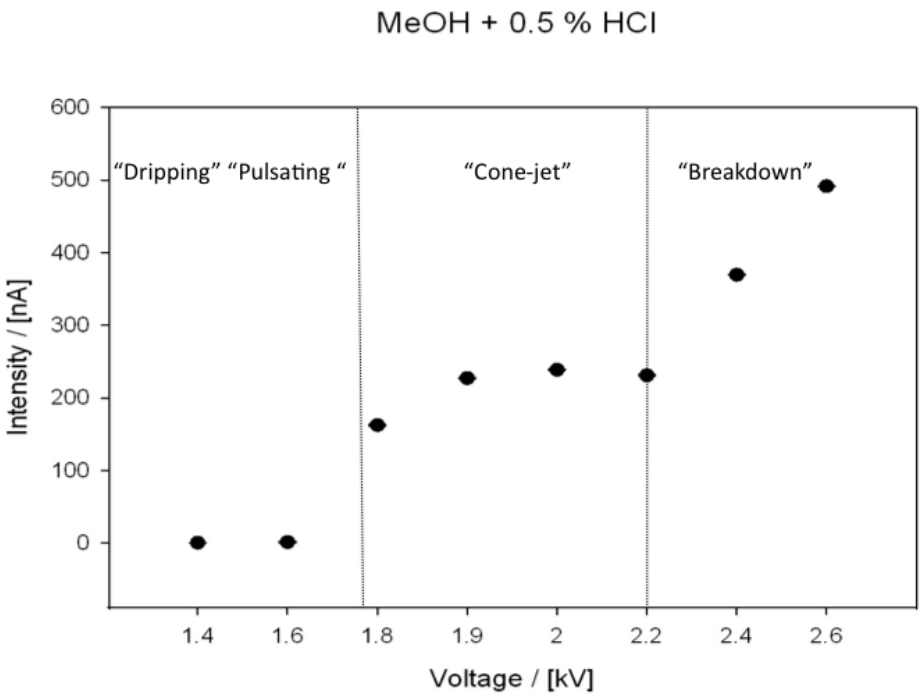

Figure 4.10: Intensity versus voltage curves at low voltages for a solution of methanol containing 0.50% of hydrochloric acid.

The spraying modes observed on the experiments are described below in Figure 4.11. For the solution of 100% MeOH + 0.50% HCl, the spray modes observed are described as follows:

Dripping, pulsating area. The liquid remained at the tip of the capillary at 1.0kV and 1.2kV, Figure 4.11(a). At 1.4kV and 1.6kV, the elongated meniscus (on-axis instabilities) emerges and the spindle mode is present, Figures 4.11(b) and 4.11(c).

Cone-jet area. At 1.8kV, the liquid meniscus becomes conical at the tip and showing on-axis instabilities, Figure 4.11(d). At 1.9kV, a kind of pulsating cone-jet mode emerged, Figure 4.11(e). The cone-jet mode remained for two minutes, then the liquid was ejected. After that, the cone-jet mode was re-stablished.

Breakdown area. The intermittent multi-jet mode and off-axis instabilities are present at 2.0kV, as in previous experiments, Figure 4.11(f). At higher voltages 2.2kV and 2.4kV the multi-jet mode are observed, Figure 4.11(g). At 2.6kV the number of

jets produced is increased with the applied voltage, leading to the rim emission, Figure 4.11(h).

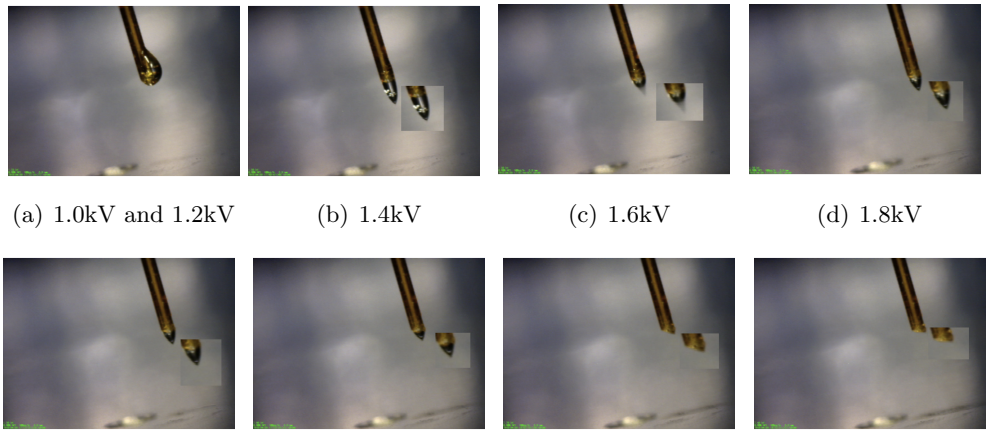

(a) 1.0kV and 1.2kV (b) 1.4kV (c) 1.6kV (d) 1.8kV

(e) 1.9kV (f) 2.0kV (g) 2.2kV and 2.4kV (h) 2.6kV

Figure 4.11: Meniscus shape for different applied voltages for the solution of 100% MeOH + 0.50% HCl. Figures 4.11(a), 4.11(b) and 4.11(c) are the ES modes observed on the Dripping, pulsating area. Figures 4.11(d) and 4.11(e) are the ES modes observed in the Cone-jet area. Figures 4.11(f), 4.11(g) and 4.11(h) are the ES modes observed on the Breakdown area. Magnification 60×

.

4.4.4 Conclusions

The onset voltage remains around 2.0kV for the three systems despite the conductivity increases. It seems that the conductivity has not any significant effect upon the onset voltage, as reported [35] by Smith. Looking at the spray current measurements, it is clear the the intensity increases as the conductivity arise, but as Smith suggested in a very weak way.

In the Table 4.6 we give the experimental conditions which lead to production of the multi-jet spraying modes for liquids with increased conductivity.

Table 4.6: Summary table of the experimental conditions which lead to the multi-jet spraying mode.

% MeOH + % HCl	Conductivity / 10^{-4} [S m^{-1}]	Multi-jet V_{onset} / kV
100% MeOH	0.7	3.5
100% MeOH + 0.10% HCl	687	2.6
100% MeOH + 0.25% HCl	1510	2.2
100% MeOH + 0.50% HCl	2100	from 2.2

The main effect observed due to the conductivity is the occurrence of the multi-jet modes at values of applied voltage only few hundreds V higher than the onset voltage. As the conductivity increases the multi-jet mode emerges at applied voltages close to the onset voltage. For the solution with the lowest conductivity the multi-jet emission appears at 3.5kV, however, for solutions containing more than 0.25% of HCl it is possible to observe the multi-jet emission at 2.2kV, whereas, the V_{onset} remains at around 2.0kV.

This effect may cause some inconveniences to the electrospray process, since it would be difficult to reach a target droplet size.

The multi-jet mode produces smaller droplets than these on the cone-jet mode, the droplets become smaller as the amount of jets on the multi-jet mode increases. As many jets emerge on the multi-jet mode it would be more difficult to control the size of the droplets.

Chapter 5

Electrospray Regimes

5.1 Introduction

As the applied high voltage increases, for steady liquid properties and flow rate, the electrospray process goes through several visual and measurable differences which are defined as spraying modes or regimes. In this chapter we describe the spraying modes observed in the proposed device.

5.2 Experimental Conditions

Applied voltage. Range 1.0–5.0kV. The voltage is increased in 0.5kV steps, and kept for 2 minutes.

Distance emitter-counter electrode. 2.8mm

Flow rate 400μL h^{-1}

ES emitter i.d./o.d. 75μm i.d./360μm o.d.

Liquid System. Methanol (LC-MS grade)

Spray modes and the spray currents are recorded.

In the Table 5.1 we describe the physical properties of the liquid used in these experiments.

Table 5.1: Physical properties of the solvent. Taken from [79].

Liquid	Density ρ/ [Kg m^{-3}]	Conductivity K / [S m^{-1}]	Surface tension γ/ [N m^{-1}]	Relative permittivity β/ (ϵ / ϵ_0)
Methanol	795	7.5e−5	0.022	33.6

5.3 Results and Discussion

In Figure 5.1, we show the plot of the spray current intensities against time. As the voltage increases, the fluctuation in the spray current increases and, as expected, different electrospray modes are observed.

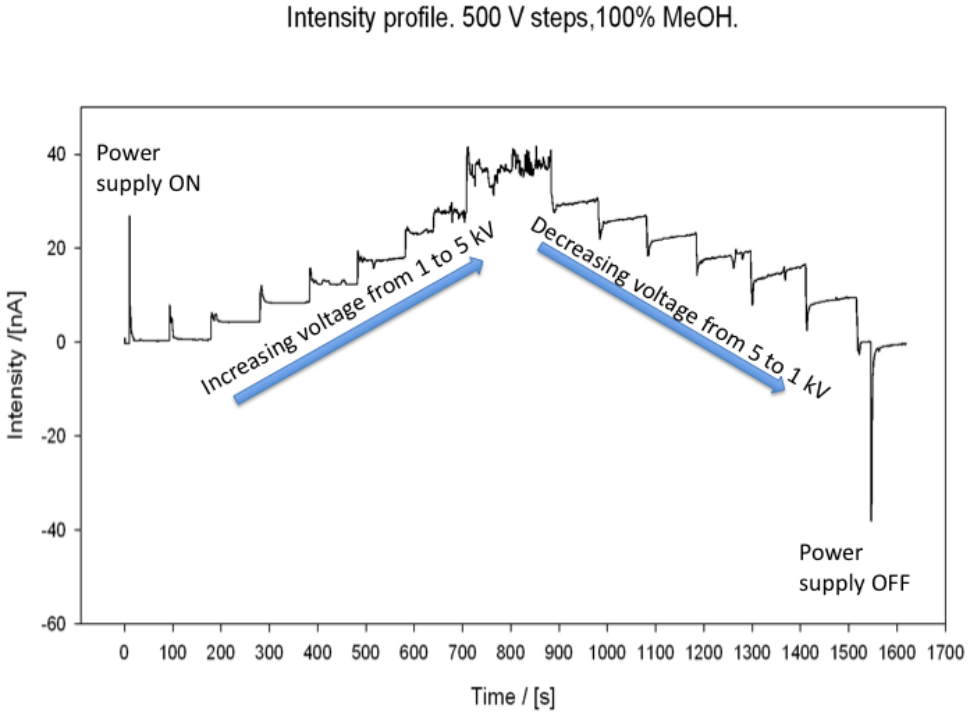

Figure 5.1: Spray current against time curve. The applied voltage increases in 0.5kV steps from 1.0–5.0kV.

The electrospray regimes are characterised from observations and spray current measurements. A diagram of the spray modes which emerged with this device is shown in Figure 5.2.

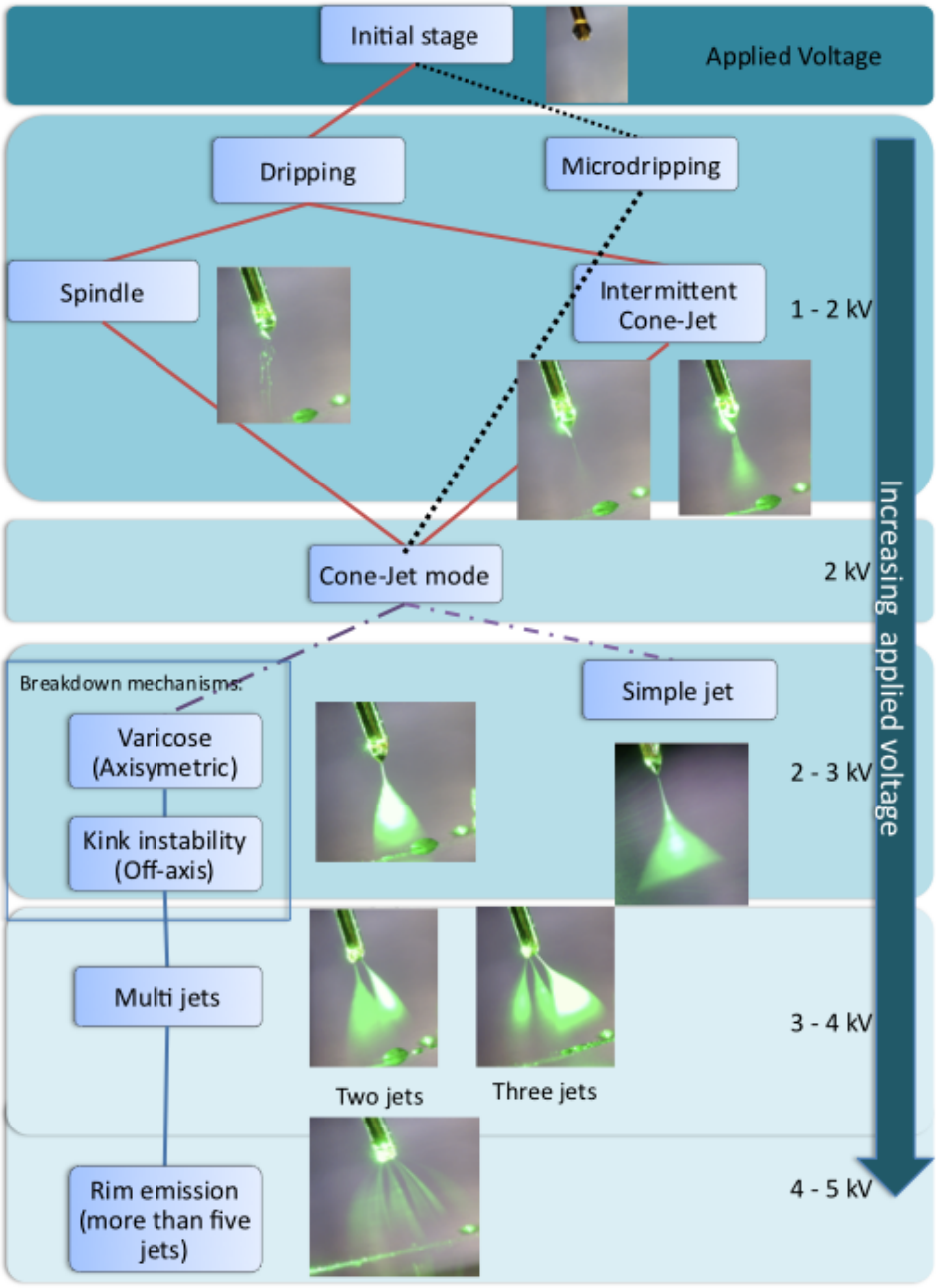

Figure 5.2: Schematic of the spraying modes observed using the developed electrospray device. Depending on the flow rate the system evolves into dripping or micro dripping modes. As the applied voltage increases, for a steady flow rate, small but perceptible changes on the liquid meniscus occur developing the electrospray modes which start with the single cone-jet mode which evolves into the multi-jet and the rim emission modes.

At the initial stage, the liquid remains at the tip of the emitter. Depending on the flow rate applied, two situations are found. If the flow rate is about 150μL h^{-1} the dripping mode appears. For lower flow rates (from 15–50μL h^{-1}) the micro dripping mode emerges. The liquid issuing from the capillary assumes the shape of a flat stable cone-like or a hemispherical meniscus. At the end of the meniscus, a single small droplet is formed. This mode can be taken as the cone-jet mode when the voltage is increased. In the case of micro dripping, the meniscus is extended by a grey blurred zone, while in the cone-jet mode, the contours of the cone and jet both appeared in black and clearly contrasted.

As the voltage increases (1.0–2.0kV), the dripping frequency increases and the dripping mode evolves into the spindle and the intermittent cone-jet modes. These modes are observed just for a few seconds. A spraying mode is considered as "unstable" when the properties of the offspring droplets are variable, and their distribution is uneven. For instance, the irregularities in the electrospray modes occur when two different spraying modes can be noticed as occurring simultaneously or alternately. This is the case of spindle, intermittent cone-jet, oscillating-jet and multi-spindle modes.

At the applied voltage of 2.1kV the cone-jet mode is achieved. The experimental verifications of the equations for the onset of the spray V_{onset}, undertaken by Smith [35] and Ikonomou [80], who reported [35, 80] that, for the stable operation of the cone-jet mode (steady conical meniscus, jet and spray), it is necessary to apply an additional "few hundred volts" above the V_{onset}. However, they did not provide a definite number. Generally, a spray mode is considered as "stable" when the cone-jet mode emerges. This mode is characterised by a conical meniscus with jet ejection and spray, and a continuous electrospray current.

As the applied voltages increases (2.5kV) the cone-jet mode breaks up, and varicose (on axis) and kink (off-axis) instabilities appear. Regarding the varicose (axis symmetric) instabilities, the jet breaks up into droplets which have similar size and sometimes accompanied by smaller satellite droplets. For slightly higher voltages (3.0kV) lateral (off-axis) or also called whipping instabilities appear. The jet stretches out into disordered bending threads and is thinned out very irregularly. It breaks up into fine droplets of very different sizes.

At applied voltages higher than 3.5kV the multi-jet mode appears. In this mode, the cone becomes smaller than that of the cone-jet mode. The jets are located close to the capillary rim (the multi-jet modes with two and three jets are depicted in the diagram).

At higher applied voltages (from 4.5kV) the multi-jet mode becomes into rim emission. Usually, the rim emission is not classified as a spraying mode, however, when more than five jets are produced in the multi-jet mode, it is considered as a rim emission. The multiple-jet modes imply observable cones and jets at each site, however in the rim emission mode the cone disappears, and the droplets seem to be issued directly from the trim of the emitter.

5.4 Conclusions

The majority of the spraying modes, emerge as the applied voltage increases. However, the oscillating-jet and precession modes do not emerge in the electrospray device tested. High flow rates and approximately 5.0–10.0mm gap between the emitter and the counter electrode (higher applied voltage is required) are required to observe these modes.

In the Table 5.2 we display the spraying modes observed.

Table 5.2: Summary of the electrospray modes observed.

Spraying mode	Voltage / [kV]	Dynamics of meniscus / jet	Flow rate / [μL h^{-1}]
Fragments of liquid (drops or spindles)			
Dripping	1.0–1.6	Axially vibrating	From 150
Micro dripping	1.0–2.0	Axially stable	Up to 50
Spindle	1.6–2.0	Axially vibrating	From 150
Liquid jets			
Cone-jet	2.0	Axially vibrating. One jet	From 150
Oscillating-jet	2.6–3.0	Oscillating cone. One jet.	From 150
Multi-jet	3.0–4.0	Stable conical meniscus. Two to five jets	From 150
Rim emission	From 4.0	More than five jets, flat meniscus	From 150

Chapter 6

CDI Sample Preparation

6.1 Introduction

The electrospray set up described in this work has been tested for particle deposition onto different substrates. These substrates are glass with different thicknesses, and silica nitride. The silica nitride windows ($500 \times 500\mu$m square, 50nm thick) are suitable substrates for the CDI experiments. The particles of interest for the CDI experiments are diatoms[1]. The samples should contain isolated particles which retained their genuine structure after being sprayed.

6.2 Experimental Set-up

As a first approach to the deposition of particles by using the electrospray device developed in this work, it has to be taken into account features such as the nature of particles, substrates, (i.e., size, solubility, hydrophobicity) and solvents (concentration, surface tension).

Regarding the solvent used to spray the particles, its surface tension should be that to reach the cone-jet mode for a given distance and applied voltage. Solvents with the lowest surface tension are advised in order to achieve the cone-jet mode at lower onset voltage.

[1] A diatom is a type of algae with walls made of silica.

Beyond the nature of particles, substrate and solvent we have also to consider the electrospray device working parameters. For instance, the distance emitter-counter electrode must be suitable for the cone-jet operation. In addition, the gap between the counter electrode and the electrospray emitter has to be convenient to enable the attachment of the substrate to the counter electrode surface and its manipulation.

The working parameters of the electrospray device to achieve the cone-jet mode are as follows:

Applied voltage. 2.0kV

Distance emitter-counter electrode. 2.4–2.8mm

Flow rate. 400μL h^{-1}

ES tip o.d./i.d. 360μm/75μm

Solvent. Methanol (LC-MS grade)

6.3 Results and Discussion: Deposition Experiments

6.3.1 Deposition of Gold Nanoparticles

In the first set of experiments, a solution of gold nanoparticles coated with a hydrophilic coating suspended in methanol is sprayed. A silica nitride window is located directly onto the aluminium plate (counter-electrode), and clamped to the plate surface by using a flange.

This approach was not successful for several reasons:

- First of all, since the window is in a fixed location on the plate, it is difficult to have the liquid-jet focused on the supported film of the substrate. This lead to the deposition onto the window (500 $\times$ 500μm square, 50nm thick) frame instead of on the supported film.
- In addition, it was not possible to reach a steady cone-jet mode before the liquid jet reached the substrate surface.

For most of the initial trials the supported film of the silicon window ends up broken at some point during the experiment because of:

- an excess of liquid coming from the tip of the capillary,

- an unstable (pulsating) electrospray cone-jet mode, and
- the silicon nitride window manipulation.

Regarding the nature of the sprayed particles and the substrate, if the particles are highly hydrophilic (coated gold nanoparticles) and the available substrate (silica nitride) is hydrophobic, the sprayed particles are prone to aggregate when they land onto the substrate surface. As a consequence, there is an uneven particle distribution. This leads to issues regarding the control of the size of the deposited particle, since it is very difficult to deposit isolated specimens. This is the case of spraying coated gold nanoparticles. As it is displayed in Figure 6.1, it is not possible to obtain isolated specimens. Even using a solution 10^{-15}M of gold nanoparticles, the particles tended to merge when they landed on the silica nitride substrate.

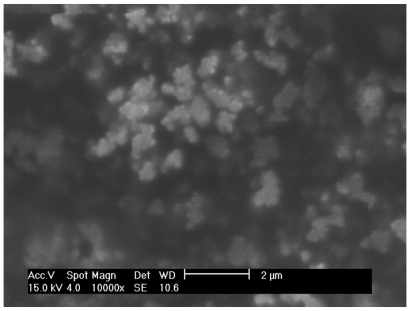

(a) SEM image of gold nanoparticles on silica nitride. Magnification 10000×.

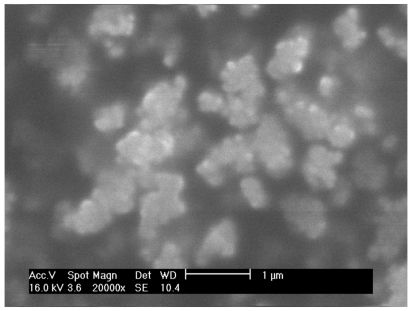

(b) SEM image of gold nanoparticles on silica nitride. Magnification 20000×.

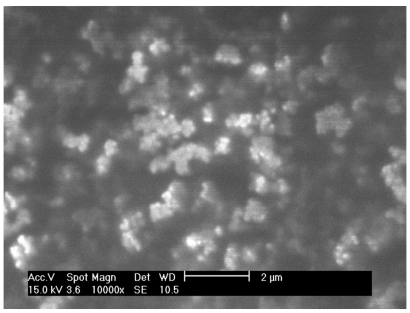

(c) SEM image of gold nanoparticles on silica nitride. Magnification 10000×.

Figure 6.1: Coated gold nanoparticles sprayed onto silica nitride. It is not possible to obtain isolated or evenly distributed specimens. The higher the similarity of the hydrophobicity of he coating and of the substrate, the higher the likelihood of an even particle deposition.

In order to avoid the direct manipulation of the silica nitride window during the experiment, it is proposed to attach it to a glass slide (24.5×76.2mm, 1.0–1.2mm thick). After that, the slide would be attached to the counter electrode.

Previously to the attachment of the silica nitride window to the slide, some deposition runs are tried on the glass slide. By using the glass slide it is observed, on one hand, that it is difficult to keep the glass slide properly attached to the aluminium plate and, it is not possible to achieve a steady cone-jet electrospray mode. Only the dripping mode is observed.

6.3.2 Deposition of Isolated Diatoms

In the second set of experiments, a glass slip is used instead of the glass slide. Despite the slips (22×40mm, 0.13–0.17mm thick) are smaller than the slides, they are still suitable for holding the silica nitride windows.

Considering the issues of having the substrate on a fixed location on the counter electrode, we must devise a mechanism to move the substrate along the plate in order to make it possible for liquid jet meet the substrate.

A couple of rigid plastic strips (approximately 10×50mm) are glued on the aluminium plate separated by 100mm. The slip supporting the silica nitride window is located in the gap between the plastic strips. The slip can be moved up and down stream.

This set up is shown in Figure 6.2.

During the experiment, the glass slip is located 1cm up stream from the emitter. The electrospray device is switched on for a few minutes in order to reach a steady cone-jet mode. When a stable cone-jet mode is achieved, the slip is slid down stream along the counter electrode in order to meet the liquid jet coming from the emitter. The device is kept spraying onto the substrate for 30s. After that, the device is switched off and the slip is removed.

Following the procedure explained previously, some samples of diatoms are sprayed onto glass slips. An aliquot of a stock suspension of diatom powder in methanol approximately 10mg L^{-1} is diluted to 0.1mg L^{-1}. This diluted suspension is used for the deposition experiments.

In Figures 6.3, 6.4 and 6.5 we display the SEM images of the diatoms sprayed onto glass slips by using our electrospray head. It is observed that the diatoms are more

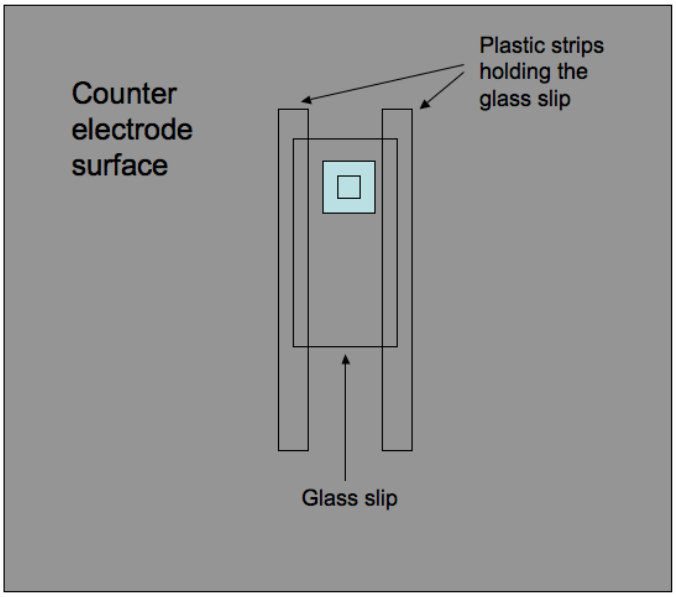

Figure 6.2: Slip set up. The glass slip is hold by a couple of plastic strips. It allows to move the slip up and down, on demand, in order to meet the liquid-jet.

evenly distributed than the gold nanoparticles sprayed previously so, it is possible to spread isolated diatoms specimens. The size of the deposited isolated diatoms or diatoms fragments is approximately 5μm.

The diatoms used in this experiment are from flea powder (DE-Sign of Nature). These specimens have different morphology and internal structure. The flea powder is diatomaceous earth made from the fossilised skeletal remains of diatoms. Each species has its own unique shape ranging from solid rod shaped to more complex structures consisting of interconnected pores [81]. Not only is imaging a diatom an important step in the development of the nanoscope, but understanding its structure at nanoscale dimensions has potential uses in both biology and photonics [82].

From these experiments particles with at least three different structures have been deposited:

- "Cigar-shaped " particles.

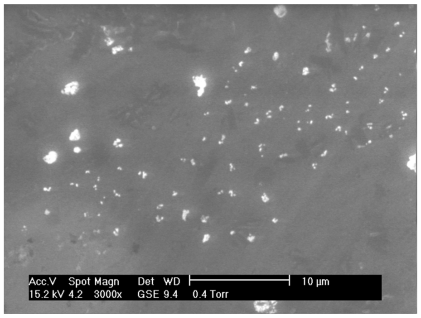

(a) SEM image of diatoms prayed on glass. Magnification 3000×.

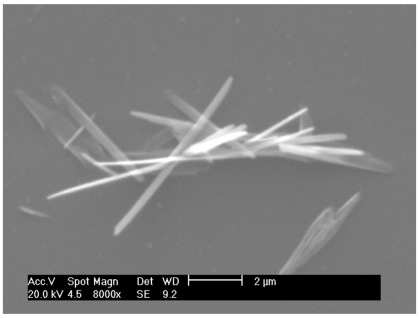

(b) Group of rod shaped diatoms. Magnification 8000×.

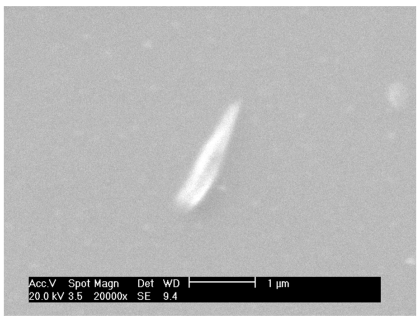

(c) Isolated rod shaped specimen. Magnification 20000×.

Figure 6.3: Diatoms sprayed onto glass cover slip. Images taken from the same area, but with different magnification. The diatoms are distributed in groups, some isolated experiments can be obtained as seen in (c)

- "Disk-shaped" particles with complex internal structure approximately 500nm ridges and approximately 100nm diameter holes in the diatom structure.

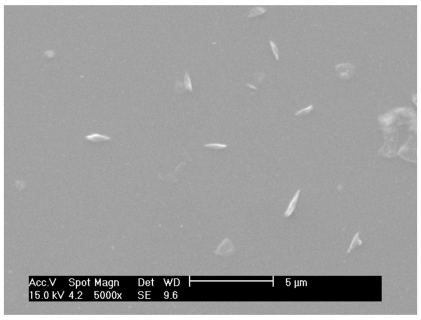

(a) Isolated rod like and round shape (background) particles are displayed. Magnification 5000x.

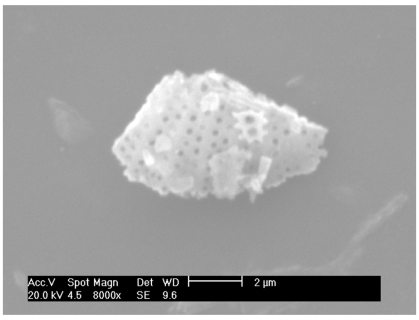

(b) Isolated fragment of a diatom complex internal structure, size approximately 5μm. Magnification 8000×.

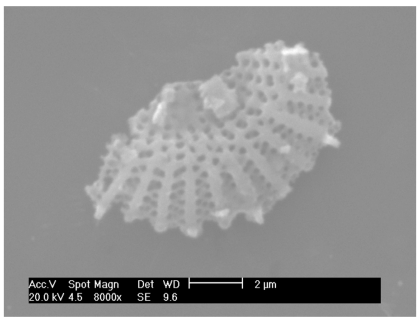

(c) Isolated fragment of a diatom with complex internal structure. Magnification 8000×.

Figure 6.4: SEM images of a diatom specimens on glass. Images taken for the same zone but with different magnification.

- Rectangular specimens with complex internal structure.

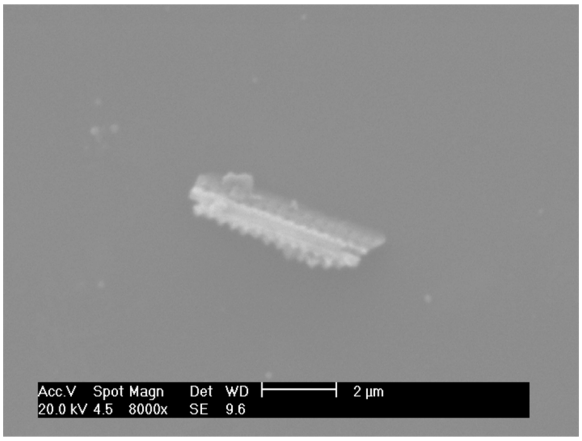

(a) Magnification 8000x.

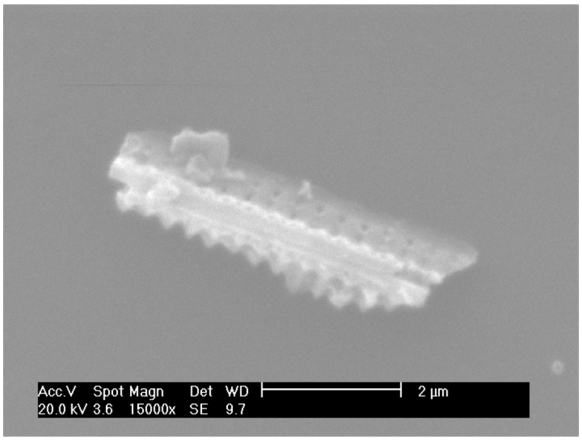

(b) Magnification 15000×.

Figure 6.5: Isolated specimen of a rectangular diatom sprayed onto a glass cover slip. Again, complex internal structure with holes and ridges. Images of the same specimen, but different magnification.

6.3.3 Coherent Diffractive Imaging Experiments

Once the set up had been tested on glass slips, silica nitride windows are used as a substrate. The silica nitride window was attached to the glass cover slip, and placed in the gap between the two plastic strips glued to the counter electrode surface facing

the ES emitter. Some diatom specimens are successfully deposited onto silica nitride substrates following the procedure described in section 6.3.2.

One of the on-demand samples produced will be used for the imaging experiment. A 10μm diameter aluminium pinhole is used to aperture the diatom specimen as seen in Figure 6.6. The silica nitride window is attached to the pinhole by using carbon tape so only one diatom is imaged, so that Fraunhofer diffraction would be observed on the CCD camera.

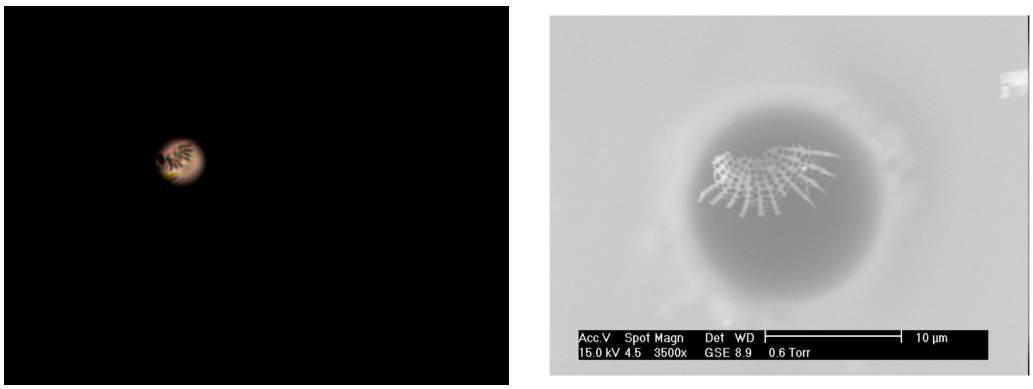

(a) Optical transmission microscope of the diatom specimen used the experiments.

(b) SEM image of the diatom. Magnification 3500×.

Figure 6.6: Optical transmission microscope image and SEM image of the diatom in a 10μm pinhole.

In Figure 6.7 we display SEM images of the diatom used in the CDI experiment.

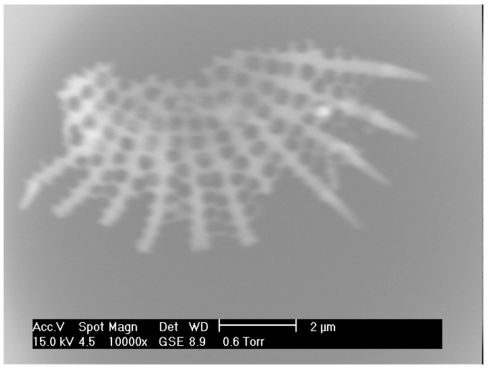

(a) SEM image details of the diatom particle. Magnification 10000×.

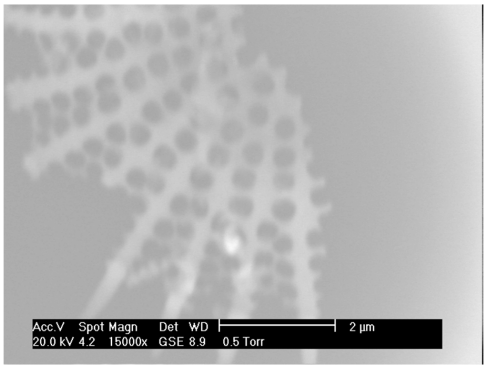

(b) SEM image details of the diatom particle. Magnification 15000×.

Figure 6.7: Visible from the SEM images are approximately 100nm diameter holes in the diatom and approximately 500nm ridges. Structure of such size is potentially resolvable using CDI with XUV radiation.

The silica window containing the specimen of diatom is placed on the sample set up of the table top nano scope. Since the diatom is made from silica, with walls of estimated thickness of at least approximately 100nm, the transmission of XUV radiation through though the diatom is $< 1 \times 10^{-3}$. As such, with the wall of the pinhole being 15μm thick and therefore blocking XUV radiation, only radiation passing inside the pinhole and around and through the open structure of the diatom will be scattered to the CCD camera. The 50nm silica nitride transmits approximately 10% of the XUV radiation of the samples.

The obtained reconstructed image is shown in Figure 6.8.

The final solution shows the object reconstruction after 6000 iterations of the algorithm. Although the crescent shape and orientation is the same as that in the microscope and SEM image, no structure on the scale below approximately 500nm was reconstructed. The algorithm was run for longer, but the reconstruction worsened.

6.4 Conclusions

For the given experimental conditions, it is possible to deposit diatoms onto silica nitride substrates. These particles retained their genuine shape and complex internal structure

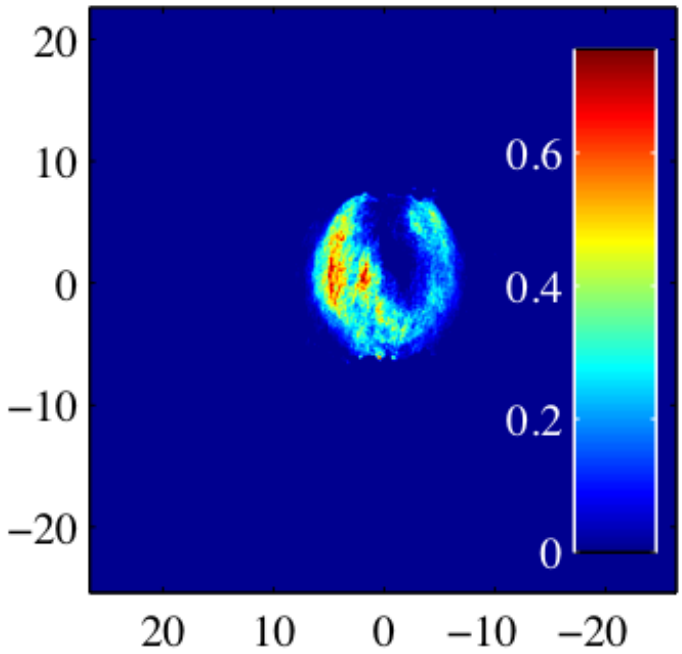

Figure 6.8: Reconstruction of the diatom image.

after being sprayed.

As explained in Section 2.2.2, the quality of the electrospray product depends on the interaction between the design (emitter-substrate distance, emitter diameter and substrate temperature) and spraying parameters (liquid feed flow rate, applied voltage) as well as solution properties (concentration, viscosity, conductivity, density and surface tension). In order to obtain an even distribution of the sprayed particles, parameters such as the hydrophobicity of the particles and the substrate have to be considered. Spraying hydrophilic particles onto hydrophobic substrates will lead to the particles aggregation, so an uneven distribution of particles.

Chapter 7

Conclusion

The configuration of the ES device comprises an electrospray emitter facing horizontally a grounded counter electrode. This configuration has been demonstrated to be valid for particle deposition onto glass and silicon nitride windows as a substrates. Alongside of this basic configuration, some peripherals such as an USB camera and a multimeter are included in order to monitor the electrospray process. in Section 3.3.3 it is stated the importance of monitoring the spray current, which can provide valuable information regarding the electrospray operation. Any irregular behaviour of the EDS, such as liquid accumulation on the counter electrode surface or an unexpected shortage on the liquid system has an effect on the spray current agains time curves. Taking a look at the curves any irregularity on the ES process can be spotted and solved in order to achieve an optimum performance. An electrospray operating in the cone-jet mode provides relatively large and stable spray current.

The device is cost effective and it can be divided in its different components. It allows to the user modify the device configuration to meet the experimental requirements. For instance the device may be used as an spontaneous Rayleigh source, if it is placed in a vacuum chamber. By modifying the emitter it may be used for making encapsulations and using different solvents hollow structures may be obtained as well.

Most of the EDSs as described in Section 2.4.2 have been designed for different applications e.g. production of films, encapsulations, etc.. However they have similarities regarding the device configuration (horizontal, vertical, single emitter, coaxial configuration) and components. In Table 7.1 are displayed the configuration details of some EDSs used in life sciences, in this table are also included the details of the ES device developed in this work.

Table 7.1: Summary/Comparison of several EDS.

Parametres	V_{Onset}	Emitter	Flow rate	Configuration	Spraying distance
Application					
PLC polymer particles with different microstructure.	8.0kV	Single emitter Stainless Steel 455μm i.d.	3.0mL h^{-1}	Horizontal grounded counter-electrode	10cm
DNA deposition.	−6.0kV	Single emitter Stainless Steel 560μm i.d. 1070μm o.d.	0.2mL min^{-1}	Horizontal grounded counter-electrode	2.5cm
Protein Bovine Serum Albumin deposition.	6.5kV	Single emitter Stainless Steel 410μm i.d. 710 μm o.d	5μL h^{-1}	Vertical nozzle-extractor system	10mm
Living Cells Electrospraying.	8.5kV	Single emitter Stainless Steel 500μm i.d.	600μL h^{-1}	Vertical nozzle-extractor system	15mm
Diatoms deposition ES device proposed in this manuscript.	2.0kV	Single emitter Fused silica 75μm i.d. 360μm o.d.	400μL h^{-1}	Horizontal grounded counter-electrode	2.8mm

The electrospray device described in Section 3.3.1 has been tested under different experimental conditions in order to optimise the ES device.

Surface Tension. As expected, it was not possible to reach the cone-jet mode with solutions whose surface tension is above the threshold value of 0.05N m^{-1} (water or other aqueous solutions of methanol).

Distance emitter-counter electrode. It was determined the optimum emitter-counter electrode distance range to enable the establishment of the cone-jet mode. This distance would be used to locate the substrate on the experiments for particle deposition. The distance ranges from 2.4-2.8mm. At greater distances the liquid remained at the emitter tip and any perceptible change was observed regarding the meniscus. for other sources, described in Section 2.4.4, the deposition of polymers is 10cm and the DNA is 2.5cm.

Emitter. Single, blunt, fused-silica capillary 75μm i.d. 360μm o.d. In other devices used for making spheres or encapsulations it is need to use a coaxial configuration.

Onset Voltage. V_{Onset} is around 2.0kV for the device described in this work [1]. However, for other devices it could be higher, around 8.0kV for the PCL structures device described in Section 2.2.2. For the experiment with DNA, the onset voltage is -6.0kV, whereas for other biological samples, such as bovine serum albumin, the stable cone-jet was achieved from 6.5kV.

Flow rate. The maximum flow rate that leads to an stable spraying mode in this device is 400μLh^{-1}.

7.1 Electrospray Advantages

- EHD has high encapsulation efficiency in comparison to wet, emulsion-based methods.
- Droplets have size smaller than those available from conventional mechanical atomisers, and can be smaller than 1μm.
- The size distribution of the droplets is usually narrow, with low standard deviation; droplets can be of equal size only for dripping and micro dripping modes, or for

[1] In practise, it is observed that it is necessary to apply a few hundreds of V more to reach an stable cone-jet mode.

Rayleigh jet breakup due to varicose wave instability.

- Charged droplets are self-dispersing in the space those results in absence of droplet agglomeration and coagulation.
- The motion of charged droplets can be easily controlled (including deflection or focusing) by electric fields.
- The deposition efficiency of charged spray on an object is much higher than for uncharged droplets.

7.2 Electrospray Limitations

- Control of a mode of spraying.
- Electrospray is very sensitive to the liquid physical properties and the electric field in the vicinity of the emitter tip. Variations on the concentration of the spraying liquid would lead to different ED products.
- One drawback to electrospray is that highly conductive solutions, such as salt solutions, may be too conductive to reach the target droplet size, since as the conductivity increases the droplet size decreases.

7.3 Electrospray Applications

- Fibre production.
- Controllable porous polymer particles generation.
- Generation of monodisperse protein nanoparticles.
- Electrospray as aerosol-based clinical therapies for pulmonary diseases.
- As photonic crystal production.
- Production of nanoparticles for drug and gene delivery.

Appendix A

A.1 Preliminary Instrumental Observations

A.1.1 Introduction

In this section we described the effect of the microscope lighting on the temperature around the electrospray device.

A.1.2 Effect of Microscope Lighting System on Temperature Around the Electrospray Emitter

Some authors [78, 83] have pointed the effect of temperature around the electrospray emitter, since liquid properties such as viscosity and conductivity depend on temperature. To avoid increasing the liquid temperature above ambient conditions they kept the lamp on only for a brief space of time, few minutes [78]. In this USB microscope the LEDs. The experiments are carried out under continuous light. In order to assess the changes on the temperature around the tip when LEDs are switched on, some continuos measurements of temperature were taken during time slots of one and two hours. The temperature sensor was located as close as possible to the tip of the capillary, the microscope was located 1cm above them. From the recorded temperatures it was concluded that the temperature around the tip never changed by more than 1°C through the studied time slot.

Appendix B

B.1 Spray Current for Different Distances Between Tip of Capillary and Counter Electrode

In the tables below are displayed the values for the averaged spray current obtained for several flow rates. The tested distances emitter-counter-electrode range from 0.4–2.8mm. These data were plotted and are displayed in Figure 4.3.

Table B.1: Spray Current measurements for 0.4mm gap

Distance 0.4 mm			
Flow rate /[μL h^{-1}]	Measurements	Intensity Mean/[nA]	Standard Error /[nA]
15.0	165	20.40	0.62
50.0	236	25.20	0.28
150.0	67	69.00	1.36

Table B.2: Spray Current measurements for 0.8mm gap

Distance 0.8 mm			
Flow rate /[μL h^{-1}]	Measurements	Intensity Mean/[nA]	Standard Error /[nA]
15.0	180	6.83	0.15
50.0	158	16.00	0.23
150.0	144	27.60	0.14
300.0	119	28.33	0.11
400.0	135	25.60	0.24

Table B.3: Spray Current measurements for 1.2mm gap

Distance 1.2 mm			
Flow rate /[μL $h^{(}-1)$]	Measurements	Intensity Mean/[nA]	Standard Error/[nA]
15.0	91	4.31	0.04
50.0	107	5.84	0.09
150.0	140	17.70	0.17
300.0	113	22.42	0.08
400.0	139	23.70	0.05
600.0	143	33.36	0.24
800.0	60	43.97	0.23

Table B.4: Spray Current measurements for 1.6mm gap

Distance 1.6 mm			
Flow rate /[μL h^{-1}]	Measurements	Intensity Mean/[nA]	Standard Error/[nA]
15.0	80	3.33	0.08
50.0	79	4.43	0.06
150.0	120	13.00	0.18
300.0	131	23.27	0.09
400.0	129	22.13	0.10
600.0	133	41.67	0.51

Table B.5: Spray Current measurements for 2.0mm gap

Distance 2.0 mm			
Flow rate /[μL h^{-1}]	Measurements	Intensity Mean/[nA]	Standard Error /[nA]
15.0	72	2.97	0.06
50.0	107	7.53	0.04
150.0	120	24.30	0.05
300.0	242	29.72	0.33
400.0	193	31.16	0.27
600.0	191	29.82	0.09
800.0	111	31.20	0.43

Table B.6: Spray Current measurements for 2.4mm gap

Distance 2.4 mm			
Flow rate /[μL h^{-1}]	Measurements	Mean Intensity /[nA]	Standard Error /[nA]
15.0	46	0.83	0.11
50.0	213	3.55	0.09
150.0	121	19.46	0.11
300.0	119	23.90	0.06
400.0	132	27.52	0.11
600.0	119	18.43	0.05

Table B.7: Spray Current measurements for 2.8mm gap

Distance 2.8 mm			
Flow rate /[μL h^{-1}]	Measurements	Mean Intensity /[nA]	Standard Error /[nA]
15.0	60	0.59	0.05
50.0	66	2.07	0.05
150.0	148	11.46	0.06
400.0	266	15.20	0.22
600.0	131	16.02	0.36
800.0	180	17.29	0.13

Bibliography

[1] Bragg W.L. The structure of some crystals as indicated by their diffraction of x-rays. *Proceedings of the Royal Society of London. Series A, Containing Papers of a Mathematical and Physical Character*, 89:248–277, 1913.

[2] Dauter Z. Current state and prospects of macromolecular crystallography. *Acta Crystallographica D*, 62:1–11, 2006.

[3] Myers H.P. *Introductory solid state physics*. Taylor & Francis, London, 1989.

[4] Pusey M.L., Liu Z. J., Tempel W., Praissman J., Lin D., Wang B. C., Gavira J. A., and Ng J. D. Life in the fast lane for protein crystallization and x-ray crystallography. *Progress in Biophysics and Molecular Biology.*, 88:359–386, 2005.

[5] Neutze R., Wouts R., van der Spoel D., Weckert E., and Hajdu J. Potential for biomolecular imaging with femtosecond x-ray pulses. *Nature*, 406:752–757, 2000.

[6] Howell M.R., Beetz T., Chapman H.N., Cui C., Holton J.M., Jacobsen C. J., Kirz J., Lima E., Marchesini S., Miao H., Sayre D., Shapiro D.A., Spence J.C.H., and Starodub D. An assessment of the resolution limitation due to radiation-damage in x-ray diffraction microscopy. *Journal of Electron Spectroscopy and Related Phenomena*, 170:4–12, 2009.

[7] Barty A., Boutet S., Bogan M. J., Hau-Riege S., Marchesini K., Sokolowski-Tinten S., Stojanovic N., Tobey R., Ehrke H., Cavlleri A., Dustere S., Frank M., Bajt S., Woods B. W., Seibert M.M., Hadju J., Treusch R., and Chapman H. N. Ultrafast single-shot diffraction imaging of nano-scale dynamics. *Nature Photonics*, 2:415–419, 2008.

[8] Gerchberg R. W. and Saxton W. O. A practical algorithm for the determination of phase from image and diffraction plane pictures. *Optik*, 35:237–246, 1972.

[9] Fienup J. R. Phase retrieval algorithms: a comparison. *Applied Optics*, 21:2752–2769, 1982.

[10] Deutsches Elektronen-Synchrotron. Free Electron Laser FLASH. `http://flash.desy.de/`Accessed at: 26th March 2014.

[11] Deutsches Elektronen-Synchrotron. `http://www.desy.de/` Accessed at: 1st April 2014.

[12] SLAC National Accelerator Laboratory Linac Coherent Light Source. `https://portal.slac.stanford.edu/sites/lcls_public/Pages/Default.aspx` Accessed at: 31st March 2014.

[13] Diamond Light Source. `http://www.diamond.ac.uk/Home.html` Accessed at: 26th March 2014.

[14] Chapman H.N., Barty A., Bogan M. J., Boutet S., Frank M., Hau-Riege S.P, Marchesini S., Hajdu J., and et al. Femtosecond diffractive imaging with a soft-x-ray free-electron laser. *Nature Physics*, 2:839–843, 2006.

[15] Wu Y., Duong A., Lee L.J., and Wyslouzil B.E. Nanoparticles for drug/nucleic acid delivery. In Dr. Abbass A. Hashim., editor, *The Delivery of Nanoparticles*. Intech, 2012.

[16] Mancuso A.P., Aquila A., Borchers G., Giewekemeyer K., and Reimers N. Scientific instrument single particles, clusters, and biomolecules (spb). Technical report, European X-Ray Free-Electron Laser Facility GmbH, 2013.

[17] Grant-Jacobs J. A. *Table-top XUV Nanoscope*. PhD thesis, University of Southampton. Faculty of Physical and Applied Sciences. Optoelectronics Research Centre, 2011.

[18] Zeleny J. The electrical discharge from liquid points, and a hydrostatic method of measuring the electric intensity at their surfaces. *The Physical Review*, 3:69–91, 1914.

[19] Zeleny J. Instability of electrified liquid surfaces. *The Physical Review*, 10:1–6, 1917.

[20] Salata O.V. Tools of nanotechnology: Electrospray. *Current Nanoscience*, 1:25–33, 2005.

[21] Gaskell S. J. Electrospray: Principles and practice. *Journal of Mass Spectrometry*, 32:677–688, 1997.

[22] Cech N. B. and Enke C. G. Practical implications of some recent studies in electrospray ionization fundamentals. *Mass Spectrometry Reviews*, 20:362–387, 2001.

[23] Castro S. and Bocanegra R. Water-based compound taylor cones held in vacuum: Feasibility and application to colloidal propulsion. *Applied Physics Letters*, 88:123105–1 – 123105–5, 2006.

[24] Jaworek A. Electrospray droplet sources for thin film deposition. *Journal of Materials Science*, 42:266–297, 2007.

[25] Gamero-Castano M., Aguirre de Carcer I., de Juan L., and Fernandez de la Mora J. On the current emitted by taylor cone-jets of electrolytes in vacuo: Implications for liquid metal ion sources. *Journal of Applied Physics*, 83:2428–2434, 1998.

[26] Gamero-Castano M. The structure of electrosprays beams in vacuum. *Journal of Fluids Mechanisms*, 604:339–368, 2008.

[27] Kebarle P. A brief overview of the present status of the mechanism involved in electrospray mass spectrometry. *Journal of Mass Spectrometry*, 35:804–817, 2000.

[28] Taylor G. Desintegration of water drops in an electric field . *Proceedings of the Royal Society of London. Series A, Mathematical and Physical Sciences.*, 280:383–397, 1964.

[29] Cole R.B. Some tenets pertaining to electrospray ionization mass spectrometry. *Journal of Mass Spectrometry*, 35:763–772, 2000.

[30] Dole M., Mack L.L., Hines R.L., Mobley R.C., Ferguson L. C., and Alice M.B. Molecular beams of macroions. *Journal of Chemical Physics*, 49:2240–2249, 1968.

[31] Iribarne J.V. and Thomson B.A. On the evaporation of small ions from charged droplets. *Journal of Chemical Physics*, 64:2287–2294, 1976.

[32] Thomson B.A. and Iribarne J.V. Field induced ion evaporation from liquid surfaces at atmospheric pressure. *Journal of Chemical Physics*, 71:4451–4463, 1979.

[33] Nguyen S. and Fenn J.B. Gas-phase ions of solute species from charged droplets of solutions. *Proceedings of the National Academy of Sciences (PNAS)*, 104:1111–1117, 2007.

[34] Fernandez de la Mora J. Electrospray ionization of large multiply charged spices proceeds via dole's charged residue mechanism. *Analytica Chemia Acta*, 406:93–104, 2000.

[35] Smith D. P. H. The electrohydrodynamic atomization of liquids. *Institute of Electrical and Electronics Engineers (IEEE) Transactions on Industry Applications*, IA-22:527–535, 1986.

[36] Borra J.P., Ehouarn P., and Boulaud D. Eletrohydrodynamic atomisation of water stabilised by glow discharge-operating range and droplets properties. *Journal of Aerosol Science*, 35:1313–1332, 2004.

[37] Jaworek A. and Krupa A. Studies of the corona discharge in EHD spraying. *Journal of Electrostatics*, 40 & 41:173–178, 1997.

[38] Cloupeau M. and Prunet-Foch B. Electrostatic spraying of liquids in cone-jet mode. *Journal of Electrostatics*, 22:135–159, 1989.

[39] Cloupeau M. Recipies for use of EHD spraying in cone-jet mode and notes on corona discharge effects. *Journal of Aerosol Science*, 25:1143–1157, 1994.

[40] Marginean I.and Kelly R.T., Page J.S., Tang K., and Smith R.D. Electrospray characteristic curves : In pursuit of improved performance in the nanoflow regime. *Analytical Chemistry*, 79:8030–8036, 2007.

[41] Cloupeau M. and Prunet-Foch B. Electrostatic spraying of liquids: Main functioning modes. *Journal of Electrostatics*, 25:165–184., 1990.

[42] Cloupeau M. and Prunet-Foch B. Electrohydrodynamic spraying function modes: A critical review. *Journal of Aerosol Science*, 25:1021–1036, 1994.

[43] Grace J. M. and Marijnissen J. C. M. A review of liquid atomization by electrical means. *Journal of Aerosol Science*, 25:1005–1019, 1994.

[44] Jaworek A. and Krupa A. Classification of the modes of EHD spraying. *Journal of Aerosol Science*, 30:873–893, 1999.

[45] Jaworek A. and Krupa A. Jet and drop formation in electrohydrodynamic spraying of liquids. A systematic approach. *Experiments in Fluids*, 27:43–52, 1999.

[46] Juraschek R. and Rollgen F.W. Pulsation phenomena during electrospray ionization. *International Journal of Mass Spectrometry*, 177:1–15, 1998.

[47] Jaworek A. and Krupa A. Generation and characteristics of the precession mode of EDH spraying. *Journal Aerosol Science*, 27:75–82, 1996.

[48] Fenn J.B., Mann M., Meng C. K., Wong S. F., and Whitehouse C.M. Electrospray ionization for mass spectrometry of large biomolecules. *Science*, 46:64–71, 1989.

[49] Fenn J.B. Electrospray wings for molecular elephants (Nobel lecture). *Angewandte Chemie*, 42(33):3871–3894, 2003.

[50] Jaworek A. and Sobczyk A.T. Eletrospraying route to nanotechnology: An overview. *Journal of Electrostatics.*, 66:197–219, 2008.

[51] Widiyandari H., Hogan C. J. J., Yun K. M., Iskandar F., Biswas P., and Okuyama K. Production of narrow-size-distribution polymer-pigment-nanoparticle composites via electrohydrodynamic atomization. *Macromolecular Materials and Engineering*, 292:495–50, 2007.

[52] Loscertales I. G.and Barrero A., Guerrero I., Cortijo R., Marquez M., and Ganan-Calvo A. M. Micro/nano encapsulation via electrified coaxial liquid jets. *Science*, 295:1695–1698, 2002.

[53] Bocanegra R., Gaonkar A. G.and Barrero A., Loscertales I. G., Pechack D., and Marquez M. Production of cocoa butter microcapsules using an electrospray process. *Journal of Food Science*, 70:E492–E497, 2005.

[54] Moerman R., Frank J., Marijnissen J.C.M., and van Dedem G.W.K. Picoliter dispensing in wells of a micro-array by means of electrospraying. *Journal of Aerosol Science*, 30(Suppl. 1):S551–S552, 1999.

[55] Moerman R., Frank J., Marijnissen J.C.M., Schalkhammer T.G.M., and van Dedem G.W.K. Miniaturized electrospraying as a technique for the production of microarrays of reproducible micrometer-sized protein spots. *Analytical Chemistry*, 73(10):2183–2189, 2001.

[56] Moerman R., Knoll J., Apetrei C., van den Doel L.R., and van Dedem G.W.K. Quantitative analysis in nanoliter wells by prefilling of wells using electrospray deposition followed by sample introduction with a coverslip method. *Analytical Chemistry*, 77:225–231, 2005.

[57] Uematsu I., Matsumoto H., Morota K., Minagawa M., Tanioka A., Yamagata Y., and Inoue K. Surface morphology and biological activity of protein thin films produced by electrospray deposition. *Journal of Colloid and Interface Science*, 269:336–340, 2004.

[58] Kumbar S. G., Bhattacharyya S., Sethuraman S., and Laurencin C. T. A preliminary report on a novel electrospray technique for nanoparticle based biomedical implants coating: Precision electrospraying. *Journal of Biomedical Materials Research Part B: Applied Biomaterials*, 81B:91–103, 2007.

[59] Pareta R., Brindley A., Edirisinghe M. J., Jayasinghe S. N., and Lukinska Z. B. Electrohydrodynamic atomization of protein (bovine serum albumin). *Journal of Materials Science: Materials in Medicine*, 16:919– 925, 2005.

[60] Jayasinghe S. N., Qureshi A. N., and Eagles P. A. M. Electrohydrodynamic jet processing: an advanced electric-field-driven jetting phenomenon for processing living cells. *Small*, 2:216–219, 2006.

[61] Wu Y., Chalmers J. J., and Wyslouzil B.E. The use of electrohydrodynamic spraying to disperse hydrophobic compounds in aqueous media. *Aerosol Science and Technology*, 43:902–910, 2009.

[62] Pareta R. and Edirisinghe M. J. A novel method for the preparation of biodegradable microspheres for protein drug delivery. *Journal of the Royal Society Interface*, 3:573–582, 2006.

[63] Xie J. and Wang C. Encapsulation of proteins in biodegradable polymeric microparticles using electrospray in the taylor cone-jet mode. *Biotechnology and Bioengineering*, 97:1278–1290, 2007.

[64] Zhang S., Kawakami K., Yamamoto M., Masaoka Y., Kataoka M., Yamashita S., and Sakuma S. Coaxial electrospray formulations for improving oral absorption. *Molecular Pharmaceutics*, 8:907–813, 2011.

[65] Wilhelm O., Madler L., and Pratsinis S.E. Electrospray evaporation and deposition. *Aerosol Science*, 34:815–836, 2003.

[66] Huanga H., Yao X., Wu X.and Wang M., and Zhang L. Ferroelectric PbTiO thin films prepared by electrostatic spray 3 ferroelectric PbTiO3 thin films prepared by electrostatic spray deposition (ESD). *Microeletronic Engineering*, 66:688–694, 2003.

[67] Lintanf A., Neagu R., and Djurado E. Nanocrystalline Pt thin films prepared by electrostatic spray deposition for automotive exhaust gas treatment. *Solid State Ionics*, 177:3491–3499, 2007.

[68] Paine M.D., Alexander M.S., Smith K.L., and Wang M.and Stark J. P. W. Controlled electrospray pulsation for deposition of femtoliter fluid droplets onto surfaces. *Aerosol Science*, 38:315–324, 2007.

[69] Wu Y.and Clark R.L. Controllable porous polymer particles generated by electrospraying. *Journal of Colloid and Interface Science*, 310:529–535, 2007.

[70] Zeles-Hahn M.G., Lentz Y.K., Anchordoquy T.J., and Lengsfeld C.S. Effect of electrostatic spray on human pulmonary epithelial cells. *Journal of Electrostatics*, 69:67–77, 2011.

[71] Morozov V.N., Morozova T.Y., and Kallenbach N.R. Atomic force microscopy of structures produced by electrospraying polymer solutions. *International Journal of Mass Spectrometry*, 178:143–159, 1998.

[72] Weierstall U., Doak R.B.and Spence J. H. C., Starodub D., Shapiro D.A., Kennedy P., Warner J., Hembree G.G., and Fromme P.and Chapman N.H. Droplet streams for serial crystallography of proteins. *Expeeriments in Fluids*, 44:675–689, 2008.

[73] Seibert M.M., Ekeberg T., Maia F. R. N. C., Svenda M., Andreasson J., Jönsson O.and Odic D., Iwan B., Chapman N.H., Hajdu J., and et al. Single minivirus particles intercepted and imaged with an x-ray laser. *Nature*, 470:78–81, 2011.

[74] Uetrecht C., Rose R. J., van Duijn E., Lorenzen K., and Heck A. J. R. Ion mobility mass spectrometry of proteins and protein assemblies. *Chemical Society Reviews*, 39:1633, 2010.

[75] van den Heuvel R. H. H.and van Duijn E., Mazon H., Synowsky S.A., Lorenzen K., Versluis C., Brouns S. J. J., van der Oost J. Langridge D., Hoyes J., and Heck A. J. R. Improving the performance of a quadrupole time-of-flight instrument for macromolecular mass spectrometry. *Analytical Chemistry*, 78:7473–7483, 2006.

[76] Suizdak G. Probing viruses with mass spectrometry. *Journal of Mass Spectrometry*, 33:203–211, 1998.

[77] Uetrecht C. and Heck A. J. R. Modern biomolecular mass spectrometry and its role in studying virus structure, dynamics, and assembly. *Chemie International Edition Angewandte*, 50:8248–8262, 2011.

[78] Fernandez de la Mora J. and Loscertales I. G. The current emitted by highly conducting Taylor cones. *Journal of Fluids Mechanisms*, 260:155–184, 1994.

[79] Lide D.R., editor. *CRC Handbook of Chemistry and Physics.* CRC Press., 89th edition, 2008.

[80] Ikonomou M.G., Blades A.T., and Kebarle P. Electrospray mass spectrometry of methanol and water solutions suppression of electric discharge with SF_6 gas. *Journal of American Society for Mass Spectrometry.*, 2:497–505., 1991.

[81] Kroger N. and Poulsen N. Diatoms: From cell walll biogenesis to nanotechnology. *Annual Review of Genetics*, 42:83–107, 2008.

[82] Gordon R., Losic D., Tiffany M.A., Nagy S.S., and Sterrenburg F.A.S. The glass menagerie: Diatoms for novel applications in nanotechnology. *Trends in Biotechnology*, 27(2):116–127, 2008.

[83] Ku B.K.and Kim S.S. Electrohydrodynamic spraying characteristics of glycerol solutions in vacuum. *Journal of Electrostatics*, 57:109–128, 2003.